Evaporative Drying of Cupric-Chloride Droplets in a Thermo-Chemical Cycle of Hydrogen Production

by

Gabriel Marin

A Thesis Submitted in Partial Fulfillment
of the Requirements for the Degree of

Master of Applied Science

in

The Faculty of Engineering and Applied Science

Mechanical Engineering

University of Ontario Institute of Technology

Oshawa

April 2008

Abstract

This thesis develops analytical and numerical solutions that predict the behavior of Cupric-Chloride droplets undergoing spraying and drying processes. Cupric-Chloride is a chemical compound with the formula $CuCl_2$ and is present as a molten salt and slurry within the Copper-Chlorine thermo-chemical cycle for generation of hydrogen. Utilizing low-grade waste heat from nuclear or other industrial sources to assist in drying of Cupric-Chloride can result in increased efficiency of the overall process. Existing drying technologies normally operate at high temperatures that make their application to a thermo-chemical process for generation of hydrogen unattractive from the perspective of energy consumption. This thesis identifies parameters that can facilitate the utilization of low-temperature heat applied to a conventional drying process. Analytical correlations for heat and mass transfer are developed and applied to the analysis of a solution of Cupric-Chloride, subject to various drying conditions. The analysis takes a single droplet of $CuCl_2$ solution in a continuum drying media. The validation of the model involves comparisons with experimental data from previous studies of different fluids on the basis of non-dimensional analysis. This thesis shows that it is possible to accomplish considerable drying through differentials of humidity alone. It also shows that the benefits of flashing the solution to enhance drying are relatively minor, and in some cases disadvantageous, when compared to the rate of evaporative drying in the spraying process. The study provides new information about the effects of different concentrations of water in the $CuCl_2$ slurry drying at low air temperatures.

TABLE OF CONTENTS

List of Figures

List of Tables

List of Symbols and Abbreviations

A	Surface area of droplet	m^2
a	Calculation constant	--
B	Mass transfer number	--
b	Calculation Constant	--
Bi	Biot Number	$\frac{hL_c}{k_d} = Nu\left(\frac{k_g}{2k_d}\right)$
c	Concentration of solids in droplet	kg $CuCl_2$ / kg H_2O
CCd	Cupric-Chloride Droplet	--
C_D	Drag coefficient acting on droplet	--
CDRC	Characteristic Drying rate Curve	--
CDRP	Constant Drying Rate Period	
CFD	Computational Fluid Dynamics	--
C_g	Vapor concentration in air	mol/m^3
C_{pg}	Specific heat of air	J/kg . K
C_p	Specific heat droplet	J/kg . K
C_s	Vapor concentration on droplet surface	mol/m^3
$CuCl_2$	Cupric-Chloride	--
D_d	Droplet diameter	m
dm	Absolute mass derivative	--
D_o	Initial droplet diameter	m

D_v	Diffusivity of vapor in air	m^2/s
F_b	Buoyancy force on droplet	N
F_d	Net force on droplet	N
F_D	Drag force on droplet	N
FDRP	Falling Drying Rate Period	--
F_g	Gravity force on droplet	N
$f(y)$	First derivative	--
g	Gravity acceleration	m/s^2
h	Convective heat transfer coefficient	W/m^2. K
H	Enthalpy	J/mol
HR	Humidity Ratio	kg H_2O / kg Air
H_2O_l	Liquid water	kg
H_2O_v	Vapor water	kg
J	Calculation Constant	--
K	Calculation Constant	--
k_{avg}	Average thermal conductivity of droplet	W/m . K
k_c	Mass transfer coefficient	mol/s . m^2
k_d	Thermal conductivity of droplet	W/m . K
k_g	Thermal conductivity of air	W/m . K
Kn	Knudsen Number	$\frac{\lambda_f}{L}$
k_s	Thermal conductivity of $CuCl_2$	142 W/m . K

k_w	Thermal conductivity of water	0.58 W/m . K
L	Knudsen Physical Length Scale	m
Le	Lewis Number	$\frac{\alpha}{D_v} = \frac{\mathrm{Sc}}{\mathrm{Pr}}$
M_{air}	Molecular weight of air	g/mol
M_d	Molecular weight of droplet	g/mol
M_{H_2O}	Molar mass H_2O	g/mol
m_l	Mass of liquid	g
m_s	Mass of solids	g
Nu	Nusselt number	$\frac{hD_d}{k_g}$
$P_{sat(T_d)}$	Vapor pressure at droplet temperature	Pa
Pr	Prandtl number	$\frac{Cp_g \mu_g}{k_g}$
P	Pressure	bar
P_1	Atmospheric Pressure	bar
P_2	Pressure level above atmospheric	bar
P_s	Pressure at spraying chamber	bar
Q	Calculation Constant	--
r	Variable droplet radios	m
R	Gas constant	8.314 m^3Pa/mol . K
R_d	Droplet radios	m

Re	Reynolds number	$\frac{\rho_g (V_g - V_d) D_d}{\mu_g}$
REA	Reaction Engineering Approach	--
S	Cross sectional area droplet	m^2
Sh	Sherwood number	$\frac{k_c D_d}{D_v}$
Sc	Schmidt number	$\frac{\mu_g}{\rho_g D_v}$
SMD	Global Sauter Mean Diameter	m
SMR	Steam Methane Reforming	--
t	Time	s
t/t_T	Elapsed time Vs Total time	--
T_d	Droplet temperature	^oC, K
T_{db}	Temperature of dry bulb	^oC, K
T_g	Temperature of air	^oC, K
T_{od}	Initial droplet temperature	^oC, K
T_s	Temperature of droplet surface	^oC, K
T_{s1}	Saturation temperature at pressure P1	^oC, K
T_{s2}	Saturation Temperature at pressure P2	^oC, K
T_{wb}	Temperature of wet bulb	^oC, K
T_1	Slurry Temperature	^oC, K
T_2	Final particle temperature	^oC, K

u	Velocity of droplet	m/s
V_d	Droplet velocity	m/s
V_g	Air velocity	m/s
V_n	Net velocity of droplet	m/s
X	Moisture fraction	--
X_c	Critical moisture fraction	--
X_e	Vapor Quality	kg H_2O_v / (kg H_2O_l + kg H_2O_v)
x_w	Mass ratio of liquid	kg H_2O / (kg H_2O + kg $CuCl_2$)
x_s	Mass ratio of solids	kg $CuCl_2$ / (kg H_2O + kg $CuCl_2$)
Z	Calculation Constant	--

Greek symbols:

α	Thermal Diffusivity	m^2/s
μ_g	Dynamic viscosity air	Pa . s
μ_d	Dynamic viscosity droplet	Pa . s
ρ_g	Density of air	kg/m^3
ρ_a	Density of droplet	kg/m^3
λ	Evaporation constant	--
λ_f	Knudsen mean free path	m
θ	Zenith / polar angle	radians
ϕ	Azimuth angle	radians

v_s	Fraction of sprayed volume	--
v	Kinematic viscosity	m^2/s

Acknowledgements

This thesis began as a question: Can water from a $CuCl_2$ slurry be efficiently removed using low temperature waste heat from a nuclear reactor?

Support of this research from Atomic Energy of Canada Ltd. and the Ontario Research Excellence Fund is gratefully acknowledged.

In truth, my co-supervisors Professor G. Naterer, and Professor K. Gabriel contributed substantially to keep the text readable and technically correct within the context of interest, providing the benefit of their criticism.

The unconditional advice of Dr. Z. Wang, and Dr. V. N. Daggupati of the two-phase laboratory of UOIT is also gratefully acknowledged.

The completion of this effort could not have been possible without the continuous support of my wife Mimi and the patient understanding of my daughters Isabella and Valentina.

1.0 Introduction

Hydrogen is a promising future energy carrier because its oxidation does not emit greenhouse gases that pollute the environment and contribute to climate change. The predominant existing technologies for hydrogen production extract hydrogen from fossil fuels, such as Steam Methane Reforming (SMR). A UOIT initiative in collaboration with Atomic Energy of Canada Ltd, Argonne National Laboratory and other partners is examining a Copper-Chlorine cycle for thermo-chemical water decomposition to produce hydrogen, thus using water and heat rather than fossil fuels to generate hydrogen. The cycle splits water into hydrogen and oxygen through intermediate Copper and Chloride compounds and chemical reactions. The chemical reactions form a closed internal loop that re-cycles all chemicals on a continuous basis, without emitting any greenhouse gases externally to the atmosphere.

Within the cycle, $CuCl_2$ is present as a solution / slurry product from the electrolytic separation of CuCl into solid Copper and aqueous $CuCl_2$. Drying of Cupric-Chloride is necessary, in order to generate solid particles, which are then placed in contact with high temperature steam to promote a reaction that releases HCl gas. This gas in turn reacts with a stream of dry Copper particles, releasing hydrogen in one stream and CuCl in a second stream that cycles back to the closed loop process. Fig. 1 is a simplified block diagram of the complete process. The area in a circle corresponds to the Cupric-Chloride ($CuCl_2$) drying process.

There are several potential alternatives to dry the $CuCl_2$ slurry. In this thesis, various alternatives are examined with emphasis on a low air temperature process. Beyond the drying process itself, there remains the question of how much water content can efficiently remain in the "dry" $CuCl_2$ particles. To determine the effect that water content in $CuCl_2$ particles has in the HCL and CuO-$CuCl_2$ reaction, is necessary to run experiments that measure side reactants resulting from known and variable water content in $CuCl_2$ particles. Although this aspect is beyond the objectives of this thesis, the reader can infer trends and deduce some preliminary observations from the graphics. Determining the ideal water content of dry particles for the thermo-chemical cycle requires extensive experimental validation and a detailed cost/benefit analysis, which lies outside of the scope of this thesis.

Approximately 116.0 kJ of heat is released internally within the Cu-Cl cycle (by exothermic reactions, solidification and cooling) and 267.3 kJ of heat is required (for endothermic reactions, drying and heating) for each gram of hydrogen produced [1]. If all internal heat was ideally recycled, then a net heat input of about 151.3 kJ/g H_2 would need to be supplied, of which 94.0 kJ/g H_2 represents the low-grade heat for spray drying, vaporizing moisture and heating of low-temperature solid particles and gas in the Cu-Cl cycle. With a precipitated slurry drying method such as that investigated in this thesis, the possibility of using low-grade heat adds to the potential of recycling heat from exothermic reactions inside the cycle.

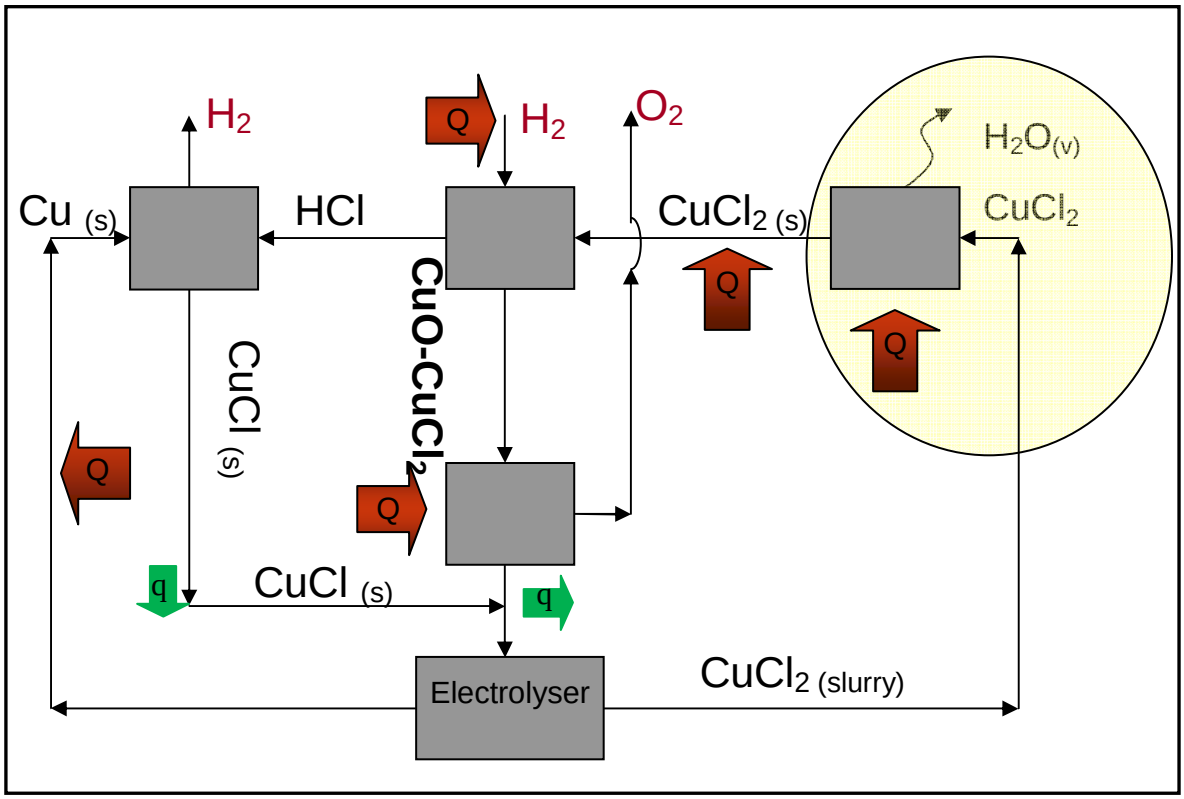

Figure 1. Simplified Schematic of a Thermo-Chemical Copper-Chlorine Cycle

Spray drying is widely used in industrial processes to obtain solid particles from slurries and solutions. The optimal design of drying processes requires analysis of the fundamental process of combined heat and mass transfer in a two-phase environment. Several approaches have been utilized by researchers and past studies described the phenomena with methods that range from pure observation [2] to analytical, and from numerical to computer assisted [3]. The majority of past research uses a single droplet approach, in order to simplify the analysis while considering all variables possible [4]. In general, researchers assume that a droplet is surrounded by a carrier phase (such as air) for which the temperature is often assumed to be unaffected by the drying process. With this assumption, effort is focused on developing an evaporation model that predicts the heating, shrinkage

and evaporation process that leads to the formation of solid particles. The analysis often considers the statistical distribution of particles and how this impacts the efficiency of the drying process, the characteristics of the solid particles and the potential of solids accumulation on the bottom of the chamber. In this thesis a single droplet approach is used to predict the behavior of $CuCl_2$ slurry, while drying in low temperature air (below 80 ^oC). $CuCl_2$ is an important fluid within the process for thermo-chemical generation of hydrogen by using heat from industrial or nuclear plants sources. Determining the feasibility of drying $CuCl_2$ by using low temperature steam has significant implications on the overall efficiency and economics of this hydrogen generation method.

1.1 Background

Several past studies have examined the spray drying of solutions, emulsions, colloidal mixtures and temperature sensitive materials [5]. Researchers have approached the problem through analytical, experimental and Computational Fluid Dynamics (CFD) modeling techniques, ranging from visual observations by Walton [2] to Lagrangian formulations by Salman et al.[3] of the drying process. Many investigators analyzed the physical phenomena of droplets in the presence of natural convection. Such experiments yielded data that was later extended to the analysis of forced convection and higher temperatures, by using a procedure that included the collection of mass and heat transfer data. One of the most relevant studies (Ranz and Marshall [4]) resulted in a correlation for determination of the heat transfer coefficient, which combines the effects of convective

mass and heat transfer from a droplet submerged in a heating media. Results were later applied to the design of industrial dryers. However, to this author's best knowledge, no previously existing papers examine the process of drying $CuCl_2$/water solutions, and none have investigated this process in relation to waste heat recovery in thermo-chemical hydrogen production. Industrial applications produce pure Cupric-Chloride through the reduction of Copper or direct chlorination of Copper and then dry the solution by using high temperature air over 150^oC The thesis addresses these issues to contribute new understanding and data related to drying processes in the $CuCl_2$ cycle.

1.2 Literature Review

Walton [2] utilized a mathematical model to analyze forced convection, mass transfer, heat conduction through the filament, and radiant heat for a single droplet suspended in a controlled air stream. The model yielded good agreement between predicted correlations and experiments. The Reynolds numbers during the experiments ranged between 27 and 100. The study monitored droplet non-sphericity and oscillation, then correlated their effects in a dimensionless group dependant on droplet viscosity, surface tension and density. Droplet temperatures were higher than those observed by Ranz and Marshall [4], and in general, variations in air velocity did not appreciably affect the droplet temperature. A linear decrease of droplet diameter with time was observed under conditions at both natural and forced convection, suggesting the transfer coefficients were independent of

droplet diameter. Under natural convection conditions, the average Nusselt number was found to be higher than the theoretical minimum of 2, by as much as 3.8.

With the exception of Salman [3], the majority of authors adopt a Lagrangian-Eulerian approach to the analysis of interactions between the droplet and the carrier phase. A purely Lagrangian approach is motivated because the evaporated volume information is lost, resulting in a strong grid dependency of the numerical solution. The Lagrangian approach resolves the vapor scales that are smaller than the flow dynamic scales. This approach results in consistent agreement between the results obtained by analytical solutions. The physical model assumes one-way coupling of momentum and continuity Equations in the vapor and dispersed phases.

Past spray drying analysis has been examined through Lagrangian-Eulerian methods and a combination of analytical methods using a coupled system of equations of momentum and continuity. The most common utilization of this analysis and practical outcome involve validating and optimizing existing industrial processes. Xu et al.[5] developed a single droplet evaporation model that does not use an analytical solution of the governing differential equations but instead simulates drying conditions by using computational fluid dynamics. At the core of the analysis is the Reaction Engineering Approach (REA) based on the assumption that evaporation is an activation process that must overcome a minimum energy barrier to proceed**.** It assumes that there is a relationship between the activation energy and the moisture content which is a characteristic property of the material under

consideration. This method's governing equation for determining the heat transfer coefficient is the correlation determined by Ranz and Marshall [4] from experimental data. It follows the more general equation that determines how rate constants vary with temperature and activation energy originally known as the Arrhenius equation. The method has a disadvantage of requiring the experimental determination of certain REA parameters, such as the activation energy and others that are often unknown.

Langrish [6] developed a characteristic drying curve and assumed that for each volume averaged value of free moisture content, there exists a corresponding drying rate, and this drying rate is proportional to the first drying period, independently of the external conditions. This concept states that the shape of the drying rate curve for a given material is unique and independent of gas temperature, humidity and velocity, This approach follows the kinetic rate law which links the reaction rate with concentrations or pressures of reactants and constant parameters. Drying rate curves for the same material at different operating conditions should be geometrically similar. This approach was found to perform well for certain ranges of air temperature, humidity and velocity for a number of materials. However, no characteristic drying curve was observed for the drying of large particles, with fibrous materials. Past data suggests that the characteristic drying curve can describe the drying of discrete particles in the range of 10 mm or smaller. This observation was confirmed through results obtained from the model developed in this thesis. The drying curves represented from the model remained geometrically similar for rates above 0.003

mg/s and within reasonable ranges of temperature, humidity and initial droplet size, but diverged dramatically with droplet sizes below 0.1 mm. and above 2 mm in diameter.

Cheng et al. [7] used a CDRC -Characteristic Drying Rate Curve- in addition to REA and performed a comparison to determine the accuracy of predictions. When using the CDRC approach, the drying process is divided into two different drying stages, such as constant drying period and a falling rate period. This method of analysis has been widely used in industry, due to its relative simplicity and ability to handle various chamber sizing parameters, while minimizing the computational effort with CFD. The method was applied to a droplet of 1.42 mm diameter with solids content of 20% to 30% and air drying temperatures above 100 ^{o}C. The experiments were conducted under varying temperature and transient conditions. It was found that the differences between the models and the experimental results were smaller for the REA than for the CDRC approach with differences ranging from 2.1% to 3.8%. The model was validated against results of experiments conducted with a single droplet suspended from a glass filament.

Huang et al. [8] developed a particle source in cell method, called PSI, which has applicability within a CFD code. Equations of the continuum carrier phase are formulated in the Eulerian mode, while the droplet Equations are formulated in a Lagrangian model. A stochastic approach is used to predict the particle trajectories, in an effort to predict the effects of a rotary nozzle design in the amount of material deposited on the walls, as well as implications on the chamber size. The model was tested experimentally on a concurrent

pilot-scale spray dryer, fitted with a rotary disc atomizer. The method can provide physical design parameters for the sizing of drying chambers. The results focused on determining velocities, axial profiles and statistical distribution of the atomized droplets and resulting accumulation of solids at the bottom of the chamber; effects that do not apply to the objectives of the Cu-Cl process in this thesis. The study determined the effects of variable parameters on the amount of dry material deposited on the walls of the drying chamber, while atomizing a milk suspension with 49% water content at 51 ^{o}C in air at 180 ^{o}C. The observations provided information on the size distribution of atomized droplets from a rotating disc atomizer. The density of the carrier phase was calculated as a function of pressure and temperature, based on the ideal gas law. Other properties such as viscosity, thermal conductivity and specific heat, were defined as polynomial functions of temperature.

In general, the drying process can be divided into sub-processes for analysis purposes. The first stage is defined as the heating of the droplet to the wet bulb temperature of the surrounding hot air. The second is defined as a stage in which the droplet is evaporating and shrinking at a constant temperature. During this stage, the concentration of solids in the droplet reaches its critical point and solid crystals precipitate on the surface of the droplet.

For the analysis of the second stage, some authors consider a receding interface with a dry core, while others correlate the drying rates to predict the behavior. The two approaches are justified on the bases of different materials with distinct thermodynamic characteristics.

They identify a constant-rate period, where fluid transport to the external surfaces occurs at a rate that matches evaporation. Then, in the falling-rate period, the fluid can no longer reach the surface at the same rate. This analysis seems to apply well in the range of 20 microns to 2 mm droplet diameters. Wang et al. [9] analyzed the drying process of aqueous multi-component colloidal ceramic suspensions by allowing them to dry on silicone paper. By varying the solid versus liquid concentration, two distinct drying regimes are obtained for distinct droplet profiles. The experiments, although not fully representative of the free-fall convective drying process of droplets, identify the drying stages and parameters that affect the different stages, among other properties of the liquid and solids it may contain. The experiments used droplets with various percentages of solids, including Zirconium Oxide and Aluminum Oxide.

Kadja et al. [10] developed a model with validation using a coal-water droplet slurry, while separating the processes into two drying stages. Coal is a hydrophobic material not likely to have much water in pores. The results indicated that the most important factor in slurry drying is the ambient temperature. The injection velocity, ambient pressure and the initial droplet temperature have little effect in the drying rate. In the first stage, a saturated liquid condition is assumed at the interface between the gas stream and the droplet. Upon reaching a critical ratio of solid to liquid, a falling drying rate stage commences. At this point the vapor diffuses first through the porous (solid) spherical shell, while the outside radius remains constant, and then the inner radius diminishes as evaporation of liquid in the core progresses. This change of the inner radius is the result of solids accumulation on the

outside crust. Validation of the model with experimental data confirmed that a two-stage method helps simplify the analysis of drying phenomena. Similarly with the Kelvin Effect, when the environment decreases slightly in super-saturation, the droplet will immediately start to evaporate and continue to do so as its radius of curvature increases.

Mezhericher et al. [11] examined drying of a motionless droplet surrounded by a flow of atmospheric air. The first stage includes initial droplet heating and subsequent evaporation from the surface at a constant rate. The second stage starts with the droplet reaching a critical moisture content and forming a dry porous solid crust of milk. The vapor, generated over the interface, diffuses through the crust pores and forms a thin boundary layer over the particle surface. From the surface, vapor is convected away by the flow of drying air. The first stage can be defined as the loss of pure water, followed by a solidification process; the second is a desorption of H_2O from the porous, solid matrix

In this thesis, drying of a $CuCl_2$ solution / slurry is analyzed for droplets with concentrations between 1 and 6 mol H_2O at 35^oC, and air at atmospheric pressure with temperatures between 75^oC and 115^oC. A mechanical nozzle is assumed to spray the slurry droplets. Pre-cooling the solution to 35^oC leads to precipitate solids and produces a slurry / solution mixture, from which the solution component eventually re-circulates and the slurry component moves to the spraying chamber. At these conditions, the slurry has a concentration of 1 to 6 mol H_2O, or 88% to 20 % $CuCl_2$, by weight. Drying of slurry at these conditions is possible by an evaporative mass and heat transfer process, by spraying

the slurry into a chamber in contact with hot air. Air heats the droplets until they reach the air dew-point temperature and a process driven by mass transport or diffusion of water vapor in air, begins until the droplet reaches a critical water concentration.

This thesis focuses on the implications of a low-temperature, heat recovery utilization alternative to conventional drying techniques that normally operate at high temperatures. The possibility of using low-grade waste heat from industrial processes for hydrogen production opens promising alternatives to the generation of clean energy. This thesis investigates the potential benefits of combined flashing and spraying of slurry in the drying process. Unlike past studies, drying of slurry droplets is examined, particularly to determine the behavior of such solutions / slurries, drying times, evaporation rates and droplet sizes, when the slurry atomizes in a low-temperature drying medium.

A literature survey of spray drying processes and their applicability to the $CuCl_2$ process indicates a need of further research in this field. Apart from cryogenic sprays, past publications refer to processes that operate in the range of 100^oC to 300^oC [3-10]. This implies heat transfer driven drying phenomena. In other aspects of the past literature, there is little emphasis on the impact of the initial droplet water concentration and the impact of changes in the drying media. This thesis considers these aspects in the drying process.

A low temperature cryogenic spray for cooling human skin was analyzed and an evaporation model was developed by Aguilar et al [12]. The model performs an analysis of

a single droplet in a simplified manner. The analysis assumes a single-phase flow in the nozzle, with subsequent droplet evaporation at the tip of the nozzle. The analysis starts from the initial conditions of the droplet, which are assumed equal to the conditions at the tip of the nozzle. Empirical correlations for evaporation of water droplets are utilized. A single droplet evaporation model involving a phase-change heat transfer analysis is developed to relate the evolution of fundamental spray variables, including diameter, temperature and velocity. A progressive scan camera is used to take photographs of the spray. With this information, the initial velocity of the droplet is determined and used to initiate a combined iterative and integral solution of the governing Equations. The model assumes a Reynolds number between 50 and 450 and uses it to initiate iterations starting from a balance of forces acting on the droplet. The corresponding drag force is calculated and the instantaneous velocity Equation is obtained. The heat transfer coefficient is calculated from the Ranz and Marshall correlation [4]. There is reasonably good agreement between the proposed model and the experimental data, in determining the evaporation rate. Of the three parameters in the model, it was found that the velocity has the least influence on the cryogenic droplet evolution.

Yang et al. [13] investigated both experimentally and theoretically the effect of heat conduction through a fiber that supports a single droplet, while exposed to a drying medium. Their analysis neglects natural convection and radiation absorption by the droplet. Experimental measurements are presented to demonstrate the effects of heat transfer through the support fiber on droplet evaporation. The heat and mass transfer rates are

determined by the same correlation used by previous models. Assume that the rate at which heat is transferred inside the droplet is substantially higher than the rate at which heat is removed from the droplet's surface. If the relationship between these two rates is equal or less than 0.1, it will be assumed that there is no temperature gradient inside the droplet and a lumped capacity heating process can be applied. This characteristic of the droplet is called the Biot number.

With a Biot number on the order of 10^{-2}, a one-dimensional transient model is used to describe the conduction input through the fiber, based on the assumption that the temperature distribution in the fiber is one-dimensional. Droplets analyzed lied in the range of 0.7 mm to 1 mm and air temperatures were between 100^{o}C and 290^{o}C.

Huang et al. [14] simulates the condition of an industrial spray dryer by using Computational Fluid Dynamics (CFD). An important assumption of the model is no agglomeration, collision or breakup among the droplets. This assumption sets the analysis on grounds similar to the single droplet model. A small Biot number is calculated for the droplets under investigation. It is assumed that no spatial temperature gradient exists within the droplets. Also, it is assumed that the particle remains spherical in shape and that two drying periods appear during the process. The periods are defined as CDRP (constant drying rate period) and a FDRP (falling drying rate period). The results of the model were compared against measurements in an industrial dryer operating with different nozzles for a variety of spray rates. The evaporation rate predicted is smaller, if the mean droplet

diameter is increased and the droplet size distribution becomes broader. This occurs because the large droplets need longer residence times before they dry completely. A lower evaporation rate results in a higher outlet temperature and net energy consumption increase.

Eslamian et al. [15] developed a mathematical model for the evaporation of nano sized solution droplets. The model attained a final particle size and wall-thickness in terms of temperature, pressure and initial solution concentration. The droplet is assumed to remain at constant temperature during the shrinkage stage. The model also assumes that the droplet is isolated, and that the heat of crystallization is small enough to be neglected. In the analysis, the continuum assumption is invalid between $0.1 < Kn$ (Knudsen number) < 10. Parameters that affect the mean free path of molecules in the continuum (air) or the droplet diameter affect the transport Equations. The experimental results identified three zones of temperature change: Initial rapid heat-up; relatively flat evaporation zone at the wet bulb temperature; and final ramp-up due to the reduction of vapor pressure because of the increase in the solute concentration. The model also indicated that the effects of the interaction with a non-continuum leads to a reduced droplet evaporation rate.

Fu-Yu et al. [16] modeled changes in the solution before the formation of a crust in a spray pyrolysis process. The modeling assumed that the flow of gas is laminar and there are no interactions between the droplets; the relative velocity between the aerosol droplets and the carrier gas is zero; that the gas surrounding the droplets follows the ideal gas law and that the temperature of the droplet is only a function of time, given the small Biot number. It is

also assumed that the droplets are spherical and that changes of concentration inside the droplet are symmetrical. A frame of reference is chosen in the center of the droplet and the mass, momentum and heat transfer processes are described accordingly. The problem then becomes a non-linear moving boundary problem, for which the solution transforms to a fixed boundary problem, redefining the variables in dimensionless form. The simulated results indicated that the movement of species inside the droplet was a consequence of diffusion and convection. Decreasing the concentration of the initial solution reduced the size of resultant particles. The effect of humidity in the surrounding air was found to be small.

Farid et al. [17] developed a model in which four drying stages are identified. The droplet was assumed to undergo a sensible rapid heat input period with no mass change. Then the droplet experiences shrinkage, with no temperature or phase change, but constant mass loss, followed by a period of crust formation with a significant change in droplet mass and temperature, then finally a short period of sensible mass heating. The model accounts for temperature variations within the droplet. The validation and results show that the drying rate is controlled by the droplet diameter and the crust thermal conductivity, and also by the air heat transfer coefficient. The model was validated against experimental data obtained with droplets of colloidal silica, with 30% water content and diameters between 1.6 and 1.8 mm. The development of this model, Equations and correlations, as well as the combined iteration and numerical solution methods do not diverge substantially from those used by other researchers in past literature.

Patel et al. [18] identified three modeling approaches based on the assumptions related to heat and mass transfer during air drying of small droplets. The first approach assumes that there is a negligible temperature non-uniformity inside a droplet and that the lumped kinetics model can be used. This approach predicts the changes in temperature and moisture concentration satisfactorily for small droplets under the laboratory conditions. This approach is widely used in modeling of large-scale operations, mainly due to the simplicity (as it requires only time integration) and fairly reasonable accuracy in the predictions of the drying parameters and product quality.

The second modeling approach assumes a uniform temperature within the small droplets, but solves the detailed moisture concentration distribution. The internal mass transfer is considered a rate limiting factor, assuming the internal heat transport occurs quickly in comparison to the internal mass transport. This approach was found to correlate the experimental weight loss data reasonably well with the theoretical predictions. The model developed in this thesis prioritizes the internal mass transfer over the heat transfer process, when there is a small temperature differential in the system.

The third modeling approach takes into account the spatial temperature distribution inside a droplet and assumes the formation of solid crust from a preferential site, usually the droplet surface. As drying proceeds, the crust is assumed to thicken and form a moving boundary or receding interface, as the liquid mass in the droplet reaches a critical point.

Birch et al. [19] developed a model that uses a population balance, in which droplets constitute the discrete phase and they are distributed into temporary compartments, determined by the residence time inside the drying chamber. The model uses constitutive Equations to describe the droplet drying mechanism. In a parallel approach, a three-dimensional model is based on the time averaged Navier-Stokes Equations. Results are compared to obtain a better understanding of the spray dryer operation. A co-current spray dryer is set to atomize droplets of milk emulsion through a rotating atomizer, with four orifices of 2.4 mm diameter. The experiments confirmed that the droplets reach the wet bulb temperature at $0.01\ s < t < 0.02\ s$ and the crust starts to form almost immediately afterwards, initiating the water evaporation period.

Brenn et al. [20] developed an analytical solution of the diffusion equation for a spherical domain with the surface shrinking linearly with time. The model can predict the morphology of the dried particles. However, the field of application is limited to salt solutions or substances with very low vapor pressure. The observations confirmed that variations in the liquid feed temperature have only marginal influences on the drying result. The evaporation rate is determined by the Sherwood number imposed convection of the droplet in its surrounding medium. The mass transfer inside the droplet is controlled by diffusion and shrinkage of the droplet surface. The liquid exhibits a Lewis number (Le) of 100 which means that temperature changes occur much faster than mass diffusion. In the

calculations, the droplet temperature is set equal to the wet bulb temperature of air at the relative humidity chosen.

2.0 Physical Process Analysis

2.1 Flashing Process

Flashing jets form as a consequence of liquid contained at conditions above the ambient saturation pressure and temperature. They are released to a lower pressure environment. At those conditions, the liquid lies in a superheated state and non-equilibrium vapor generation occurs during liquid flashing, when the pressure suddenly drops [21], [22].

As fluid travels through a nozzle, an external heat source heats the liquid between T_{s1} and T_{s2}, and the pressure is mechanically increased from P_1 to P_2 , while remaining at saturated conditions (see line A-B in Fig. 2). During the heating process, the saturation temperature is lower than the corresponding saturation temperature at the given pressure.

As soon as the liquid enters a lower pressure environment, an approximately iso-enthalpic flashing process occurs (line B-C in Fig. 2) and the result is a mixture of vapor and liquid inside the P-H curve. Smaller droplets vaporize instantaneously, while bigger droplets evaporate only partially and the remaining liquid rains out through a cloud to create a pool at the bottom of the spraying chamber.

If the chamber pressure is below P_1 (atmospheric pressure), additional flashing occurs and the process continues until the saturation temperature at such pressures is reached (see point D in Fig. 2).

Atomization processes (line B-D in Fig. 2) are cited in the literature as approximately iso-enthalpic [15]. Based on this assumption, the location and energy content of a droplet at point D are unknown values, given that the droplet diameter decreases from the time it starts to interact with the surrounding air.

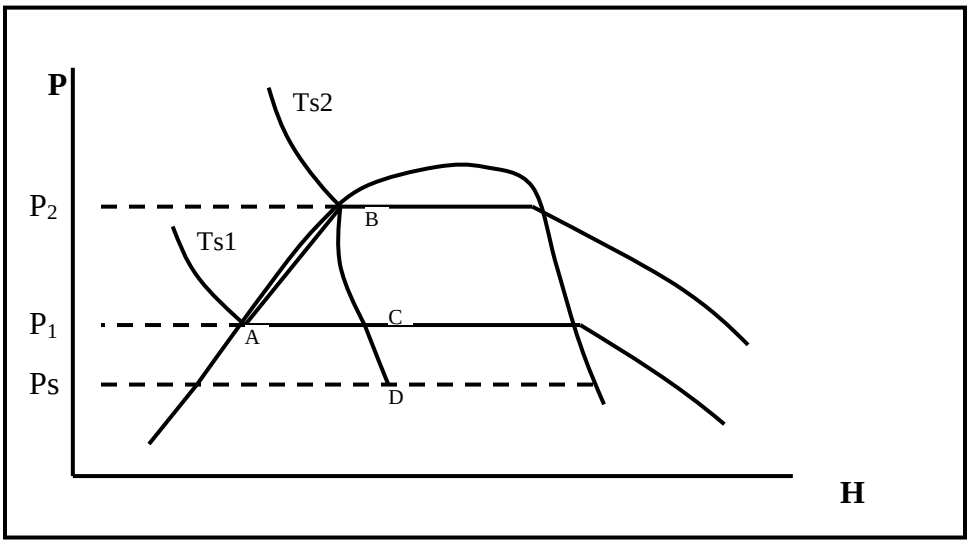

Figure 2. Pressure-Enthalpy Diagram of Flashing Process –ABCD-

One alternative to improve the efficiency of spray drying processes involves combined flashing/spraying of the hot solution (after heated and pressurized from electrolyser output conditions) into a chamber at atmospheric pressure, where it enters into contact with air

preheated at a temperature above the solution temperature. The flashing effect evaporates water instantaneously out of the solution into a cloud. The surrounding air absorbs a substantial amount of water in this initial stage [21].

Flashing effect that results from a sudden pressure change have been previously studied in the context of hazardous fluids, where the sudden rupture of containers or pipes can result in the formation of explosive clouds and liquid pools.

Cleary et al [21], analyzed the large-scale release of a liquid contained at upstream conditions above its local atmospheric boiling point. The authors presented a detailed experimental investigation with hazardous, liquefied gases, while simulating flashing conditions. The analysis found that "small droplets" ($D_d < 150$ µm), which represent the larger number of droplets, only represent 0.5 to 17 % of the mass, and the large droplets account for the complement, i.e., 83 to 99.5 % of the mass. Whether a release occurs under sub-cooled or superheated conditions, rainout of larger droplets creates a spreading vaporizing pool in the vicinity of the release orifice, and establishes the amount of material that remains airborne as the cloud disperses.

The process that follows depends on the local conditions of the surrounding media, and the resulting drying time is similar to that of a pure spraying process, under a given temperature/mass differential. This evaporation process becomes the driver and hence determines the time that the solution requires in contact with air to dry the droplets,

independently of the original flashing conditions. In this situation, the larger droplets, which dry most slowly, are the limiting portion of the spray and they determine the ultimate chamber dimensions.

A direct consequence of flashing is that the amount of liquid to evaporate is potentially reduced. Therefore, the overall efficiency of the process is higher, since less energy is required to evaporate water. But the drying time required to dry the bigger droplets is larger, increasing the size of the equipment.

Investigations of flashing effects typically focus on modeling of incidents that have involved pipe ruptures in pressurized water reactors (PWR). The objective of this thesis is to predict the consequences of the phenomena in pipe flow, due to a pressure drop, as well as safety implications for the reactor.

In a flashing process, the stream exiting from a nozzle consists of finely atomized droplets and liquid droplets. They both experience instantaneous vaporization, although to different magnitudes. Smaller particles (order of 30 μm or less) vanish as their critical mass evaporates. Larger droplets evaporate from the surface to the extent that their vapor pressure reaches equilibrium with the environment. Low superheat levels tend to result in a breakup that occurs due to aerodynamic forces. High superheat levels result in droplet growth and breakup, which dominates over aerodynamic breakup [20]. The vapor mass production rate vanishes when the dryness fraction reaches its unconstrained equilibrium

value [21]. The flashing effect for a liquid particle terminates when its local vapor quality, X, defined as the ratio of liquid content to vapor content, reaches the equilibrium vapor quality, X_e [23]. Low superheat levels tend to result in breakup that occurs due to aerodynamic forces. High superheats result in droplet growth and breakup, dominating over aerodynamic breakup.

A correlation for the droplet-size distribution has been developed based on the Rosin–Rammler size distribution as presented in Eq. 1. The Rosin–Rammler correlation provides a model for estimating the droplet size distribution in sprays, with $v(D_d)$ representing the volume of flashed liquid. Cleary et al. [21] represented the correlation in terms of the droplet global Sauter Mean diameter (SMD) as follows:

$$1 - v_s(D_d) = \exp[-0.3(D_d/\mathrm{SMD})^{1.6}] \quad (1)$$

The Sauter Mean Diameter is defined as the diameter of a droplet that has the same volume to surface area ratio as the total sprayed sample. The SMD provides a reliable way of establishing the average diameter of droplets in a given spray sample.

If one selects a critical droplet size, above which all liquid released will rain-out, the percentage of the total volume of spray that rains out can be directly determined (see Fig. 3). Past studies found through experimental and analytical means that the volume contained in

droplets with diameters of 100 μm or less is negligible for the range of initial conditions. Droplets above 100 μm will rain out and contribute to the convective drying load.

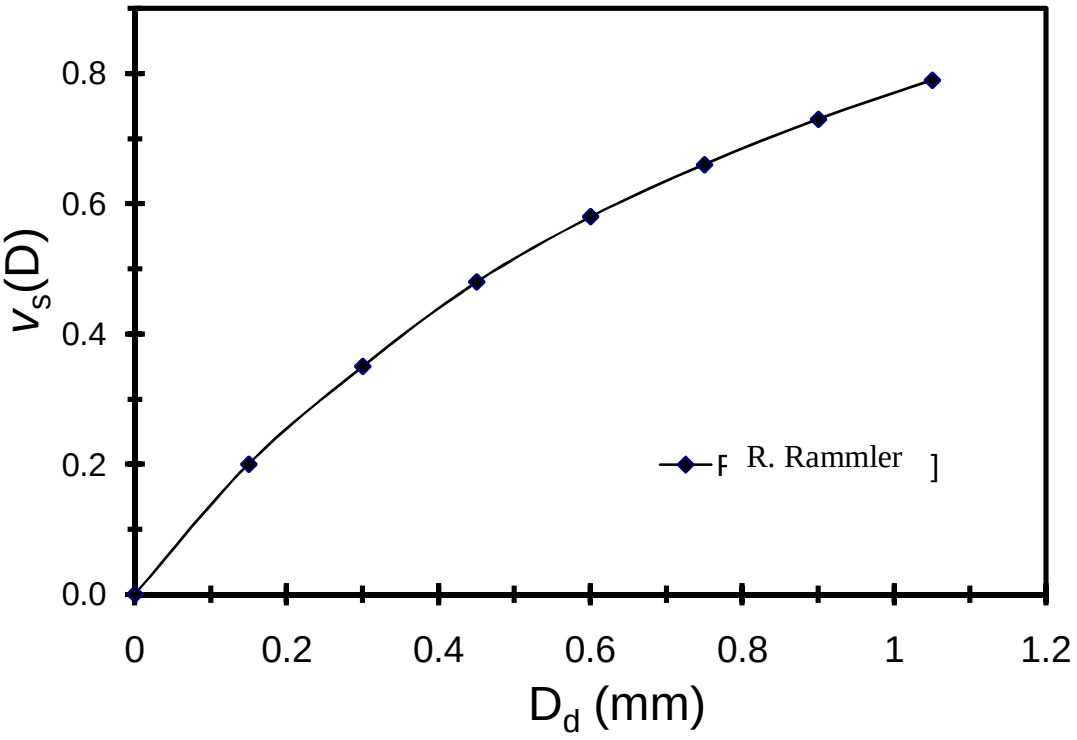

Figure 3. Droplet Diameter vs. Fraction of Total Volume of Spray [8]

Flashing occurs from an instantaneous pressure drop in a liquid at conditions above saturation, for a given final pressure, lower than the pressure at the nozzle. As discussed previously, flashing phenomena occurs in various engineering problems, such as leaks of hazardous materials from pipes at high pressure [23]. An important factor in the design of safety measures to deal with leaks is to determine the amount of liquid in the cloud (flashed liquid), versus the amount of rained out liquid.

Past studies have generally found that the amount of liquid that evaporates as a consequence of flashing is usually small, compared to the rained out liquid. The results suggest that the flashing effect will have a minor benefit for the $CuCl_2$ drying process**.**

2.2 Spraying Process

Several past studies have been conducted on the evaporation of water and solution droplets, in contact with a gas-heating medium. From those studies, several useful empirical correlations exist to predict the droplet evaporation rate, based upon the initial droplet conditions and characteristics of the carrier phase. Most studies have focused on droplets submerged in a continuum, under quiescent conditions, without accounting for convection effects. Fig. 4 is a schematic diagram of a typical co-current spray drying arrangement.

Through numerous drying processes tested with particles moving at different velocities, Ranz and Marshall [4] generated empirical correlations that account for the convective effects on droplets moving with respect to the surrounding media. The experiments investigated the factors influencing evaporation rates of liquid droplets consisting of pure solutions and liquids with suspended solids. The research concluded that the mass and heat convective processes can be represented with similar correlations for heat and mass transfers. The correlations define the Sherwood number (**Sh**) for mass transfer as a function of the Reynolds (**Re**) and the Schmidt (**Sc**) numbers; and the Nusselt number (**Nu**) for heat

transfer as a function of the Reynolds number (**Re**) and the Prandtl number (**Pr**). The correlations are shown in detail with Eq. 15 and 16 (to be presented in Chapter 4).

Aguilar et al. [12] investigated the effects of cryogenic fluids evaporating in atmospheric air, by developing a single droplet evaporation model. The analysis includes phase change evaporation and it correlates the evolution of droplet parameters, such as temperature, diameter and velocity. The liquid initially at sub-cooled conditions in the nozzle, atomizes into a lower pressure environment, where it evaporates while absorbing heat from the surrounding atmosphere.

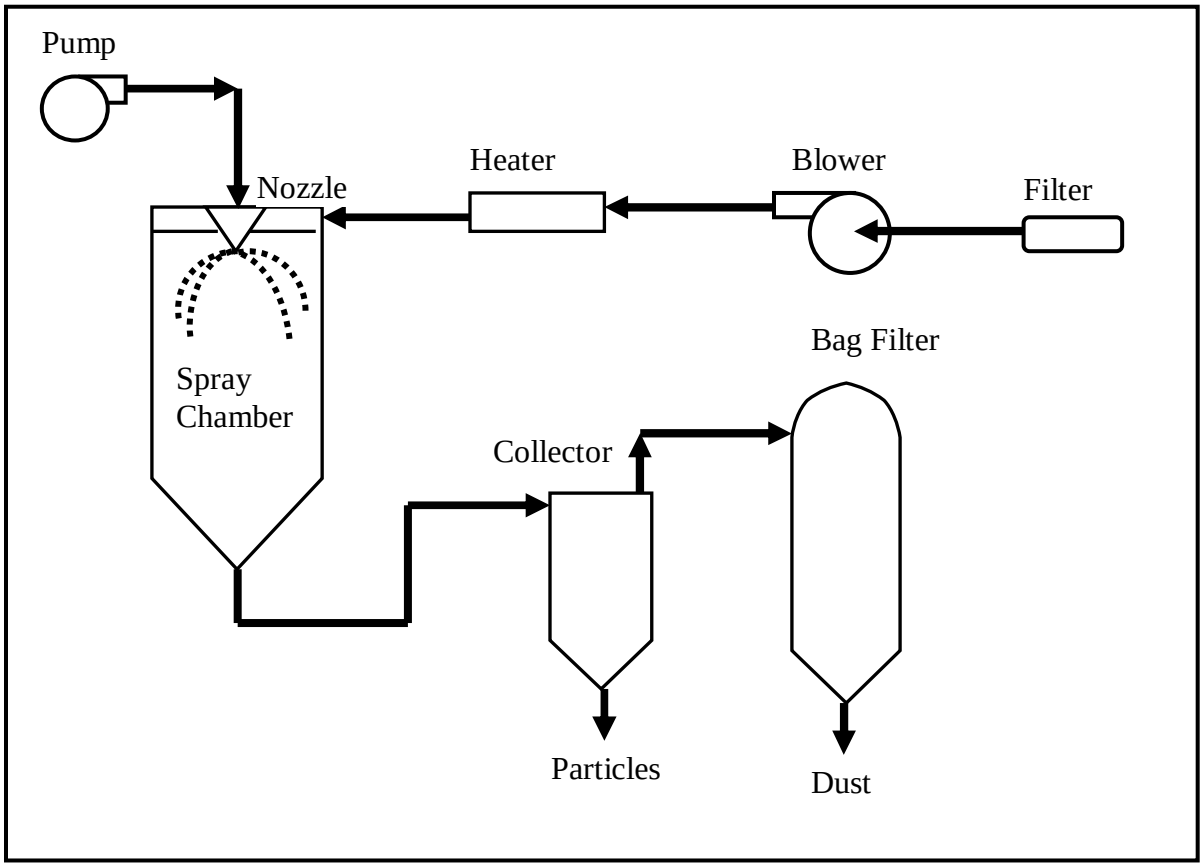

Figure 4. Schematic of a Co-Current Spray Dryer System

In order to obtain meaningful results, a combination of theoretical models, extrapolation of experimental trends and fitting of the predicted dependencies to the experimental data was used. Then, predictions of droplet diameter evolution as a function of distance traveled, away from the nozzle, initial droplet velocity and diameter, were produced.

Spray drying is a well-known method of drying and it is used in a a large number of applications for products ranging from foods to mineral ores and chemicals. It is an efficient means of drying, due to the large surface area available for heat and mass transfer, as a result of atomizing the liquid into very small droplets of the order of a few hundreds of microns [17]. In general, it can be assumed that the two-phase flow is dilute; i.e., compared with the volume of the drying medium, the particle volume occupies a very small fraction.

A spray drying analysis often uses the assumption that both external convection and internal conduction control the drying process. The hot air heats the droplets (line A-B in Fig. 5) until the liquid reaches the saturation point at atmospheric pressure. At this point, evaporation starts and continues (line B-C in Fig. 5), as long as the heating temperature is higher than the saturation temperature of the liquid at atmospheric pressure, or the partial vapor pressure of the surrounding air is lower than that of the vapor on the droplet surface. Under the later conditions, the critical water content of the droplet becomes the limiting factor in the evaporation process.

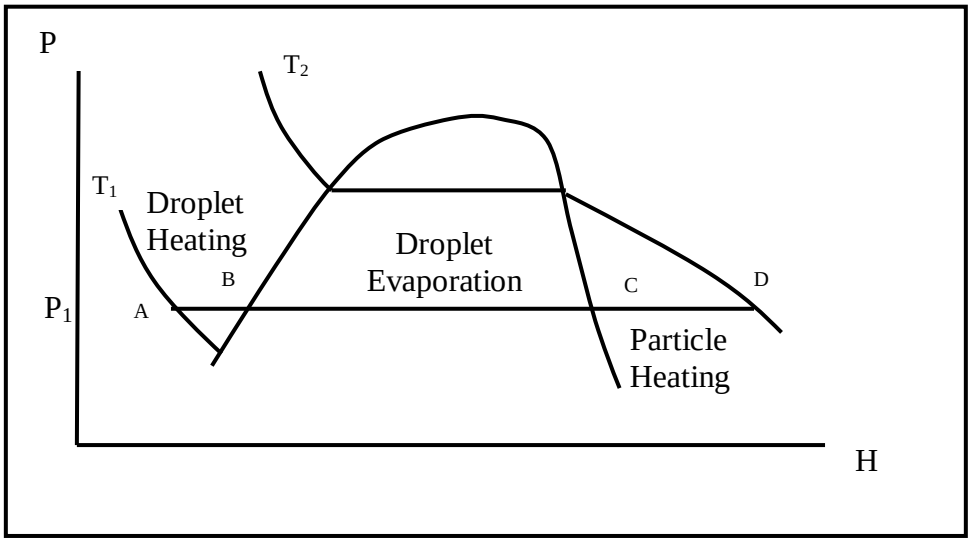

Figure 5. Phase Diagram of a Spraying Process–ABCD-

Evaporation continues at a constant temperature until point C is reached. A further temperature increase occurs as the solids in the droplet are heated to a temperature close to the dry bulb temperature of the surrounding air. Spraying the solution into contact with atmospheric air at low temperatures, under a mass transfer driven process requires a significant vapor concentration differential between the droplet surface and surrounding air. This situation typically makes the drying rate substantially slower.

Another drying alternative considered in this study is combined flashing / spraying into a chamber at atmospheric pressure, in contact with air preheated at a temperature above the solution/slurry temperature. The results will provide an insight into the effects of temperature, humidity, velocity of the continuum and the drying rate of droplets.

The droplets evaporate, subject to the temperature differential between droplets and air. The heat transfer becomes a driving process and determines the time that a solution requires in contact with air. Since the temperature differential is low, the drying time is substantially longer than a high-temperature drying process. In this situation, larger droplets, which dry more slowly, are the limiting portion of the spray process and they determine the chamber dimensions.

A direct consequence of flashing/spraying is that the remaining amount of liquid to evaporate via convection can be potentially less than a pure spraying process. Therefore, the overall efficiency of the process is potentially higher, since less water needs to evaporate, so the heat consumption may be less. This assumption is valid, as long as the volume of liquid flashed is substantial. A considerable amount of liquid does not vaporize and it flows out of the cloud in the shape of droplets that rain out and dry through a mass / heat transfer diffusive process. The length of duration of this process becomes the driving parameter for the overall drying phenomena, hence eliminating the benefit of the initial instantaneous flashing of a portion of liquid.

By contrast, during a spray drying process, droplets (order of 100 μm or more) enter the chamber at an ambient temperature and evaporate through a convective heat and mass transfer process, driven by the drying media (usually hot air). A solid particle eventually deposits at the bottom of the chamber.

In the next chapter, a predictive formulation is developed to analyze the spraying phenomena described in this section. In the analysis, it will be assumed that mass and momentum changes of the dispersed droplets do not contribute to that of the drying gas. Since the mass of the droplet is small, when compared to the mass of the continuum, it is assumed that kinetic energy changes in the drying air due to droplet movement, are negligible. Furthermore, given the continuous cycling of carrier gas (air) in spray dryers, the analysis assumes that the drying air remains at constant temperature and humidity conditions.

The majority of past papers assume a process whereby after continuous evaporation, an external, thin core forms and solidifies, while providing a porous medium through which the remaining water evaporates. This approach provides an ideal frame for numerical solutions, since the formation of a tiny core becomes the initial condition, from where calculations can start. The new proposed method in this thesis focuses on the time required for full evaporation of the liquid contained in the droplet. Since the droplet contains both solids and liquid, evaporation of liquids is the focus of analysis. Therefore, evaporation results in a continuous shrinkage of the droplet, with no solid core formation, but rather a continuous growth of $CuCl_2$ crystals. Under this approach, the average thermal conductivity of the droplet remains nearly constant.

The process depicting the drying stages is shown in figure 6. A droplet at a temperature lower than that of the wet bulb temperature of the air enters the chamber at point 1. A fast

heating process occurs, as the droplet temperature reaches the air dew point temperature. During this period, no evaporation occurs. Assume that the rate at which heat is transferred inside the droplet is substantially higher than the rate at which heat is removed from the droplet's surface.

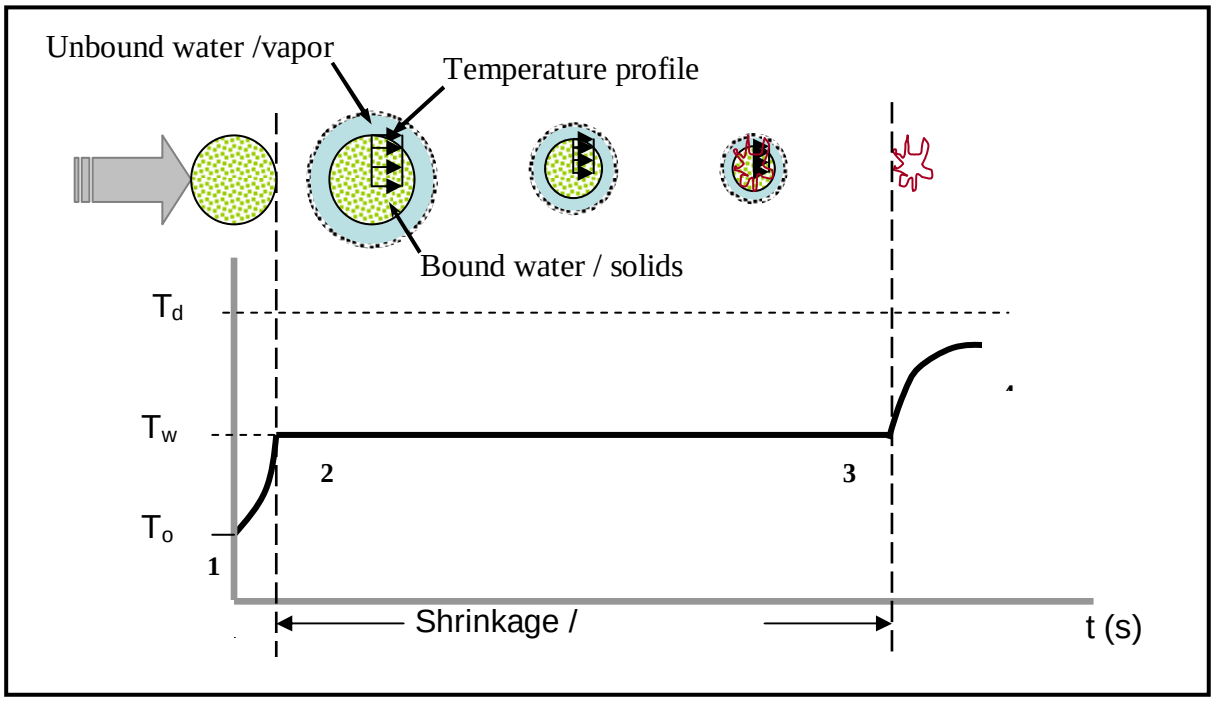

Figure 6. Stages of a Spray Drying Process

If the relationship between these two rates is equal or less than 0.1, it will be assumed that there is no temperature gradient inside the droplet and a lumped capacity heating process can be applied. This characteristic of the droplet heating process is called the Biot number. Since the Biot number is small, it is assumed that the droplet has a uniform temperature.

This approach simplifies the analysis and eliminates the need for an internal temperature profile in the evaporation equation.

Between points 2 and 3 in figure 6, the droplet remains at a constant temperature and the evaporation process occurs. Evaporation continues until the liquid has been removed and random crystals of solid start to grow. At point 3, the crystals continue to gain heat and the drying process ends with the particle deposited at the bottom of the chamber.

3.0 Formulation and Solution Procedure

3.1 Initial Heating

In the first stage of drying, 1-2 in figure 6, the temperature of the droplet increases to reach the air wet bulb temperature. Furthermore the model makes the assumption that the droplet is spherical with isotropic physical properties, and that the droplet temperature changes only in the radial direction [10]. The following energy Equation in spherical polar coordinates governs the heating process,

$$\rho_d C_p \frac{DT_d}{Dt} = k_d \nabla^2 T_d + \mu_d \left(\frac{\partial u}{\partial r} \right)^2 \tag{2}$$

where

$$\nabla^2 T_d = \frac{1}{r^2} \frac{\partial}{\partial r} \left(r^2 \frac{\partial T_d}{\partial r} \right) + \frac{1}{r^2 \sin(\theta)} \frac{\partial}{\partial \theta} \left(\sin(\theta) \frac{\partial T_d}{\partial \theta} \right) + \frac{1}{r^2 \sin^2(\theta)} \frac{\partial^2 T_d}{\partial \phi^2} \tag{3}$$

$$\frac{DT_d}{Dt} = \frac{\partial T_d}{\partial t} + v \frac{\partial T_d}{\partial r} + \frac{v_\theta}{r} \frac{\partial T_d}{\partial \theta} + \frac{v_\phi}{r \sin(\theta)} \frac{\partial T_d}{\partial \phi} \tag{4}$$

It is assumed that internal convection within a particle is negligible, due to the small diameter and as a consequence, the second, third and fourth terms in Eq. 3 and 4 are assumed negligible. Then, Eq. 2 simplifies to:

$$\rho_d C_p \frac{DT_d}{Dt} = k_d \frac{1}{r^2} \frac{\partial}{\partial r}\left(r^2 \frac{\partial T_d}{\partial r} \right) \tag{5}$$

$$\frac{\partial T}{\partial t} = \frac{\alpha}{r^2}\left[\frac{\partial}{\partial r}\left(r^2 \frac{\partial T}{\partial r} \right) \right] \tag{6}$$

The initial condition at $t = 0$ is defined by the droplet initial temperature as follows:

$$T = T_o \tag{7}$$

For boundary conditions, the temperature at the centre of the droplet changes as a function of time only, so

$$\frac{\partial T_d}{\partial r} = 0, \text{ at r} = 0 \tag{8}$$

The temperature change of the droplet occurs from the interaction with air and it is a function of the heat transfer coefficient and of thermal conductivity of the droplet [25]. At the outer surface of the droplet,

$$-k_d \frac{\partial T_d}{\partial r} = h(T_s - T_\infty), \text{ at } r = R_d \quad (9)$$

A solution of the governing equation for droplet temperature, subject to initial and boundary conditions, will show that heating of the droplet occurs in a short time, on the order of tenths of a second.

3.2 Temperature Distribution

Following the initial heating process, the droplet experiences a process of shrinkage in which the temperature is approximately uniform. In the second stage, evaporation occurs from the droplet surface. This behavior has been confirmed through several experimental measurements [8], [27] and it is reasonable assumption for the analysis of stage 2-3, evaporation and shrinkage, in figure 6.

The uniform temperature assumption is confirmed through the Biot number of the droplet. If the droplet satisfies the following condition [25],

$$\mathbf{Bi} = \frac{hL_c}{k_d} < 0.1 \quad (10)$$

The error associated with using the lumped capacitance method is small. For a droplet diameter in the range of 1 mm, the Nusselt number is approximately 2.5. In order to estimate the Biot number, the following Equation is used:

$$\mathbf{Bi} = \frac{hL_c}{k_d} = \mathbf{Nu}.\left(\frac{k_g}{2k_d}\right) \tag{11}$$

where k_g and k_d are the thermal conductivity of air and droplet respectively.

The thermal conductivity of a droplet, consisting of a combination of $CuCl_2$ and water, is defined as:

$$k_{av} = x_w k_w + x_s k_s \tag{12}$$

where k_s and k_w represent the thermal conductivity of $CuCl_2$ and water, respectively. The fractions x_w and x_s are calculated by using the condition of minimum void fraction for packing of spherical particles [11],

$$x_s = \frac{V_l}{(V_v + V_s)} \tag{13}$$

Due to the high Copper content in cupper chloride, the combined thermal conductivity of the slurry, k_{av}, is about 150 *w/mK*. Since k_g = 0.024 *w/mK*, the Biot number from Eq. 11

and 12 is approximately 0.003. Therefore, the temperature within the droplet is approximately uniform (lumped capacitance approximation is valid).

3.3 Mass Transfer Process

The solution approach will analyze the spray drying process as a coupled heat and mass transfer analysis. The dilute portion (droplets) of the spray consists of a type of two-phase flow. The dispersed phase is a result of droplets flowing through the continuum [27]. The continuum air is a form of continuous gas phase. Under these assumptions, the evaporation rate of a droplet is defined as the water evaporation transfer from an individual particle to the continuum. Past literature indicates that most studies assume a high temperature of the continuum, when compared to the droplet, thus indicating a heat driven process. With a low temperature of the continuum, the process is mass transfer driven, more than heat transfer.

The Sherwood number (**Sh**) is the ratio of convective mass to diffusive mass transport. It is correlated in terms of the relative velocity between the droplet and continuum.

$$\mathbf{Sh} = \frac{k_c D_d}{D_v} \tag{14}$$

Ranz and Marshall [4] proposed the following correlation for heat and mass transfer of a spherical particle. The correlation is the result of data collected from experiments with droplets drying in air [12].

$$\mathbf{Sh} = 2 + 0.6.\ \mathbf{Re}^{1/2}\ \mathbf{.\ Sc}^{1/3} \qquad 1 < \mathbf{Re.\ Sc}^{2/3} < 5\ .\ 10^{4} \tag{15}$$

$$\mathbf{Nu} = 2 + 0.6\ .\ \mathbf{Re}^{1/2}\ \mathbf{.\ Pr}^{1/3} \qquad 1 < \mathbf{Re.\ Pr}^{2/3} < 5\ .\ 10^{4} \tag{16}$$

where Sc and Nu and Pr are the Schmidt, Nusselt and Prandtl numbers respectively defined as:

$$\mathbf{Sc} = \frac{\mu_g}{\rho_g D_v} \tag{17}$$

$$\mathbf{Nu} = \frac{hD_d}{k_g} \tag{18}$$

$$\mathbf{Pr} = \frac{Cp_g \mu_g}{k_g} \tag{19}$$

Substituting Eq. 14 in Eq. 15,

$$k_c = \frac{D_v}{D_d}\left(2 + 0.6\ \mathbf{.\ Re}^{1/2}\ \mathbf{.\ Sc}^{1/3}\right) \tag{20}$$

The driving force for evaporative mass transfer is the vapor concentration differential. The following equation describes the mass transfer diffusion rate as a function of water vapor contained in the air and droplet surface [26]:

$$\frac{dm}{dt} = k_c \pi A M_d \left(C_s - C_g\right) \tag{21}$$

where "*A*" represents the surface area of the droplet, and k_c is the mass transfer coefficient defined in terms of the Schmidt number from Eq. 20. C_s and C_g represent the vapor concentration at the droplet surface and the bulk air respectively.

Substituting in Eq. 21 and simplifying,

$$\frac{dm}{dt} = D_v D_d \pi M_d \left(2 + 0.6 . \mathbf{Re}^{1/2} . \mathbf{Sc}^{1/3}\right)\left(C_s - C_g\right) \tag{22}$$

The vapor concentration on the droplet surface is a function of the saturation pressure at the temperature of the droplet. During the shrinkage stage, the droplet is assumed to remain at the wet bulb temperature of the air.

$$C_s = \frac{P_{sat(T_d)}}{RT_d} \tag{23}$$

where R is the ideal gas constant, and,

$$C_g = X_i \frac{P}{RT_g} \tag{24}$$

Here *Xi* represents the mole fraction of water vapor in the surrounding air and it is defined by the following equation:

$$Xi = \frac{\frac{\mathrm{HR}}{M_{H_2O}}}{\left(\frac{1}{M_{air}} + \frac{\mathrm{HR}}{M_{H_2O}}\right)} \tag{25}$$

Assume that the decrease of droplet mass is proportional to the decrease of droplet diameter. Furthermore, assume that the decrease of a single droplet diameter is a function of time, as given by the "D_2 law" [13]:

$$D_d^2 = D_0^2 - \lambda t \tag{26}$$

where λ is the evaporation constant determined by the mass transfer and heat transfer coefficients. The droplet mass is defined by:

$$m = \rho_d \frac{\pi D_d^3}{6} \tag{27}$$

Applying the first derivative,

$$\frac{dm}{dt} = \rho_d \frac{\pi D_d^2}{2} \frac{dD_d}{dt} \tag{28}$$

From Eq. 26,

$$\frac{dD_d}{dt} = -\frac{\lambda}{2D_d} \tag{29}$$

Substituting this into Eq. 28

$$\frac{dm}{dt} = \rho_d \frac{\pi}{4} \lambda D_d \tag{30}$$

The equation for droplet diameter under quiescent conditions can be modified to account for convection effects resulting from a moving droplet, by substituting the appropriate λ factor in Eq. 30. Using Eq. 22 and 30, the rate of change of diameter as a function of time can be obtained:

$$\frac{dD_d}{dt} = \frac{2D_v M_d}{\rho_d D_d} \left(2 + 0.6 . \mathbf{Re}^{1/2} . \mathbf{Sc}^{1/3}\right). \left(C_s - C_g\right) \tag{31}$$

where the Reynolds number is defined as:

$$\mathbf{Re} = \frac{\rho_g (V_g - V_d) D_d}{\mu_g} \tag{32}$$

The term V_g-V_d represents the relative (or net) velocity of the droplet, V_n, in air.

Substituting Eq. 32 and 17 into Eq. 31 and simplifying leads to the following expression for the rate of diameter change:

$$\frac{dD_d}{dt} = -\frac{4D_v}{\rho_d D_d} M_d (C_s - C_g) - \frac{1.2 D_v^{2/3}}{\rho_d D_d^{1/2}} \left(\frac{V_n^{1/2} \rho_d^{1/6}}{\mu_g^{1/6}} \right) M_d (C_c - C_g) \tag{33}$$

Since V_n is a function of time, Eq. 33 is a non-linear, ordinary differential Equation of the form:

$$D_d^{'}(t) = a D_d^{-1} + b D_d^{-1/2} f(t) \tag{34}$$

The initial value of droplet diameter D_o is non-zero and selected arbitrarily for testing purposes. The known information about the curve at the initial point in time is utilized and the solution is iterated over small steps of time. A marching method is utilized and the series converges when evaluated and truncated at third order. The series is evaluated iteratively with the average density of the droplet recalculated after each iteration,

starting from the velocity equation, Eq. 33. The following expression for diameter as a function of time is obtained:

$$D_d = D_0 + D'f(y) + D''t^2/2 + D'''t^3/6 \tag{35}$$

The constants and derivatives in Eq. 35 are represented by the following expressions:

$$J = \frac{-4D_v M_d (C_s - C_g)}{\rho_d} \tag{36}$$

$$K = -1.2M_d \left(\frac{D_v^{2/3}}{\rho_d}\right)\left(\frac{\rho_g}{\mu_g}\right)^{1/6}(C_s - C_g) \tag{37}$$

$$D_d' = JD_0^{-1} + KD_0^{-0.5}V^{0.5} \tag{38}$$

$$D'' = 0.5KD_0^{-0.5}V_g^{-0.5}(Z + 2Qt) + f(y)D' \tag{39}$$

$$f(y) = -JD_0^{-2} - 0.5KD_0^{-1.5}(V_d + Zt + Qt^2)^{0.5} \tag{40}$$

$$a = g + g\left(\frac{\rho_g}{\rho_d}\right) \tag{41}$$

$$b = \frac{75(\mu_g/\rho_g)}{D_0^2} \tag{42}$$

$$Z = bV_g \tag{43}$$

$$Q = b/3 + V_g \tag{44}$$

The partial water vapor pressure at the droplet surface and the vapor pressure in the drying gas are main factors determining the transport rate. The magnitude of the difference between vapor concentrations, defined by the term C_s-C_g in Eq. 33, depends substantially on the vapor pressure differential, which in turn depends on the relative humidity of the drying air. The mass transfer process is predominant between the time when the droplet reaches the air's wet bulb temperature, and the time when the droplet reaches the critical humidity content.

The drying process is characterized by a constant drying rate, followed by a falling drying rate. When the droplet reaches the critical humidity content, the drying rate starts decreasing until it becomes negligible. If the initial water content is above the critical humidity point, the initial drying rate is approximately uniform (called a constant drying rate). If the initial water content is equal or below the critical humidity content, the drying rate is decreasing (called a decreasing drying rate). Figure 7 shows the predicted drying rate curves for initial water concentrations of 1.5, 0.6, 0.1 and 0.01 mol of initial H_2O, versus 1 mol $CuCl_2$. With initial water concentrations of 1.5 and 0.6 moles, the drying rate trend is to increase or stay stable and it approximates a constant drying rate. At 0.1 and 0.01 mol, respectively, the curve's trend is a falling drying rate. Below the critical 0.6 mol initial water content, the curve's trend is a falling drying rate, from the beginning of the process.

The mass diffusion process occurs as long as the driving forces, determined by the humidity content in the droplet versus the humidity content of the surrounding air can drive the

evaporation process. The relationship between droplet solids and water content is determined by:

$$c = \frac{1}{(1+X)} \tag{45}$$

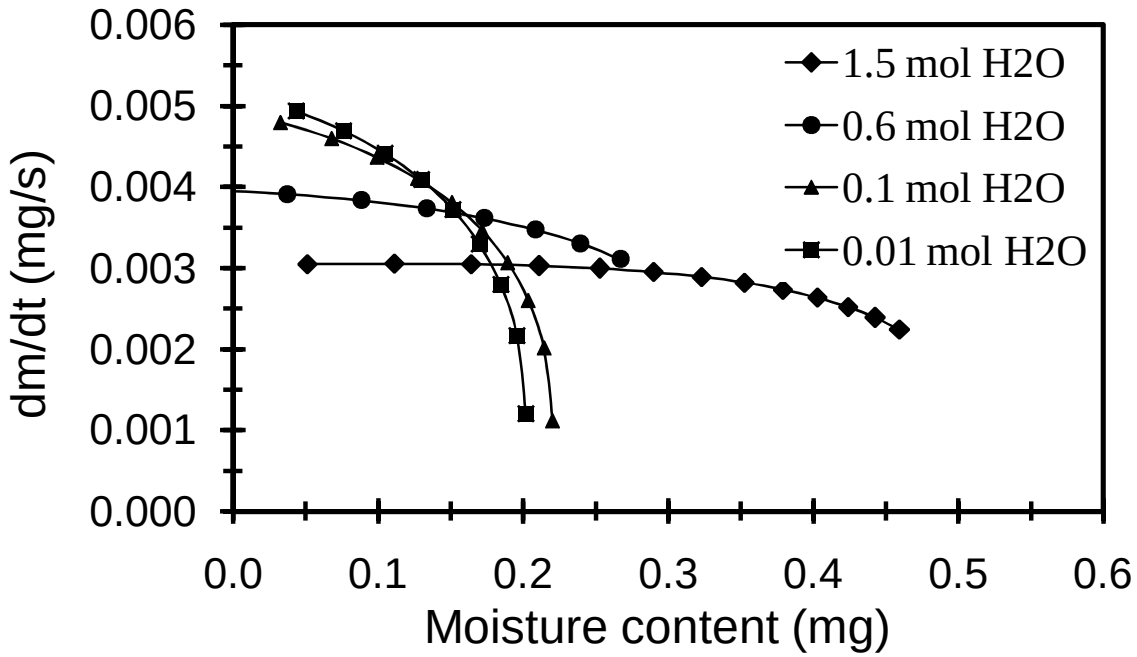

Figure 7. Evaporation Rate at Critical Moisture Content

In this Equation, X is the ratio of the mass of water content to solids content ($CuCl_2$) of the droplet, as defined by,

$$X = \frac{m_l}{m_l + m_s} \tag{46}$$

The mass transfer process from the droplet occurs at T_{wb}, and the mass diffusion process stops once the critical moisture content (X_c) is reached. Heating and evaporation continue as a result of the temperature differential between the droplet and air, in a heat transfer driven process.

3.4 Heat Transfer Process

A low temperature drying process is fundamentally driven by mass transfer, as a consequence of the diffusivity of vapor in air. This depends mainly on the differential between vapor concentration at the droplet surface and vapor in air. Conversely, if the temperature differential is significant, the evaporation rate becomes a function of the heat transfer rate as follows:

$$\frac{dm}{dT} = \frac{hA\Delta T}{\lambda} \tag{47}$$

The Nusselt number was previously defined through the Ranz and Marshall correlation as follows:

$$\mathbf{Nu} = 2 + 0.6 \,\mathbf{.}\, \mathbf{Re}^{0.5} \,.\, \mathbf{Pr_g}^{0.33} \tag{48}$$

Combining the previous equations, it can be shown that

$$\frac{dD}{dt} = \frac{-4k_g}{C_{pg}\rho_d} \ln(1+B)\left[1 + 0.3 \,.\, \mathbf{Re}^{1/2} \,.\, \mathbf{Pr_g}^{0.33}\right] \tag{49}$$

where the Reynolds number is

$$\mathbf{Re} = \frac{\rho_g (V_g - V_d) D_d}{\mu_g} \tag{50}$$

Integrating Eq. 49 over time, the drying time of the particle is obtained as a function of air humidity and temperature.

3.5 Kinetics of the Droplet

The speed of a falling droplet increases until the air resistance balances the gravity force. A buoyancy force arises from the density difference between the droplet and the carrier phase which contributes to deceleration of the droplet. Applying this force balance, the instantaneous velocity of the droplet is obtained by [20],

$$F_d = F_g - F_b - F_D \tag{51}$$

where F_d is the net resulting force that governs the droplet movement, F_g is the gravity force, F_b is the buoyancy force and F_D is the drag force.

$$F_d = m\frac{dV_d}{dt} \tag{52}$$

$$F_g = mg \tag{53}$$

$$F_b = mg\left(\frac{\rho_g}{\rho_d}\right) \tag{54}$$

$$F_D = \frac{1}{2}\rho_d S C_D V_d^2 \tag{55}$$

where S represents the cross sectional area of the droplet:

$$S = \pi D_d^2 / 4 \tag{56}$$

Substituting Eq. 51:

$$m_d \frac{dV_d}{dt} = mg - mg\left(\frac{\rho_g}{\rho_d}\right) - \frac{1}{2}\rho_d \pi \frac{D_d^2}{4} C_D V_d^2 \qquad (57)$$

Integrating the differential equation by an iterative process and a Taylor series expansion yields an equation for the instantaneous velocity. When solved in conjunction with the mass transfer rate equation, the instantaneous rate of evaporation and evaporation time for a particular initial size of droplet are obtained.

Deceleration of the droplet is a consequence of the drag force acting on the surface of the droplet. Walton [2] compiled some of the experiments performed by Ranz and Marshall [4] For droplet diameter between 0.1 to 1 mm, submerged in air in a mass transfer driven process, the Reynolds number is known to lie between 20 and 400, so the drag coefficient can be formulated as follows [8]:

$$C_D = \frac{24}{\mathbf{Re}}\left(1 + f\left(\mathbf{Re}\right)\right) \qquad (58)$$

where **Re** is the droplet Reynolds number, and *f*(**Re**) takes into account the change of drag coefficient with droplet size as follows,

$$\begin{aligned} &f\left(\mathrm{Re}\right) = a_1 \,.\, \mathbf{Re}^{b1} + a_2 \,.\, \mathbf{Re}^{b2} \\ &a_1 = 0.17 \;,\; a_2 = 10^{-6} \;,\; b_1 = 0.632 \;,\; b_2 = 2.25 \end{aligned} \qquad (59)$$

A tabulation of C_D for the range of **Re** indicates that the drag coefficient is approximately 2 for the range of Reynolds number in this thesis (To be presented in Table # 1).

Substituting Eq. 57:

$$\frac{dV_d}{dt} = g - g\left(\frac{\rho_g}{\rho_d}\right) - \frac{3}{2}\frac{V_d^2}{D_d} \tag{60}$$

A solution of Eq. 33 assumed an initial average droplet density and an initial average droplet diameter. With these average values, the first and second terms in Eq. 60 become constant and it can then be explicitly integrated by using a Taylor expansion. An Iterative process is utilized, where the original average diameter and density are revised on each iteration, after substituting the velocity Equation into the mass transfer Eq. 33. The solution uses the critical humidity concentration in the droplet, as a criterion for convergence. The iterative procedure was implemented in Matlab (see Apendix A)

4.0 Results and Discussion

In this chapter, numerical results based on new formulations developed in previous chapters, will be presented.

Fig. 8 shows a comparison of droplet mass evolution with time, as predicted by the model, versus the experimental results measured for a SiO_2 slurry. Nesic [23] conducted experiments with single droplets using several materials at various concentrations, among them silica (SiO_2) and milk. Several researchers have used Nesic's experimental data, in order to confirm their predictions, under different circumstances, with good accuracy and agreement [11].

The results from Nesic's measurements served as a useful validation for predictions. The data corresponds to experiments performed with SiO_2 droplets in hot air flowing at 1.75 m/s and 178^{o}C. SiO_2 has a dry basis density of 2500 kg/m^3. The slurry used in the experiments contains up to 30% water. The experiments used hot air with a humidity ratio of 0.01 kg H_2O / kg Air.

Comparisons between the experimental results obtained by Nesic with SiO_2, and the model developed in this thesis, predict the behavior of a 1.8 mm diameter droplet within 0.33 standard deviations. This provides a good basis from which to analyze drying of $CuCl_2$ droplets under different circumstances.

When compared to the experimental data obtained with milk, the predicted accuracy of the model decreases when the droplet approaches its critical mass at the end of the drying process. A detailed analysis of the results obtained by Nesic, using milk droplets, indicated that the assumptions of uniform temperature inside the droplet are no longer valid for this particular situation. The lumped capacity method cannot be utilized with the droplets of milk. It is expected since milk is an emulsion while SiO_2 in water is a suspension. A calculation of the Biot number confirms this observation results in a value higher than one.

The data in table 1 refers to the experimental data for SiO_2 and predictive model for $CuCl_2$.

Substance	**SiO_2**	**$CuCl_2$**	**Air (70 °C)**	**Air (178 °C)**
Density (kg/m^3)	2500	3300		
Molar Mass (g/mol)	60.08	134.45		
Specific Heat (J/mol . K) [27]	44.35	114.87	4.22	4.19
Average Density Droplet (kg/m^3)	1766	2434		
Droplet Diameter (m)	0.0019	0.001		
Dynamic Viscosity (m^2/s)			1.97	3.0
Density of Air (kg/m^3)			1.067	0.779
Thermal Conductivity (W/m . K)	0.55	280	0.029	0.037
Prandtl	0.708	0.69	0.708	0.69
Reynolds	0.00083	0.001		
Biot	0.0067	0.0001		

Table 1. Characteristics of Silica, Cupric-Chloride and Air [27]

Data from table 1 indicates that the Biot number for both processes is below 0.1 indicating that the results obtained from the model when applied to $CuCl_2$ can be properly used for predictions in various applications.

The model developed in this thesis has been applied to model the behavior of Colloidal Silica drying in air at 178°C. The model compares against the experimental results obtained by Nesic [24]. The comparison is presented in figure 8.

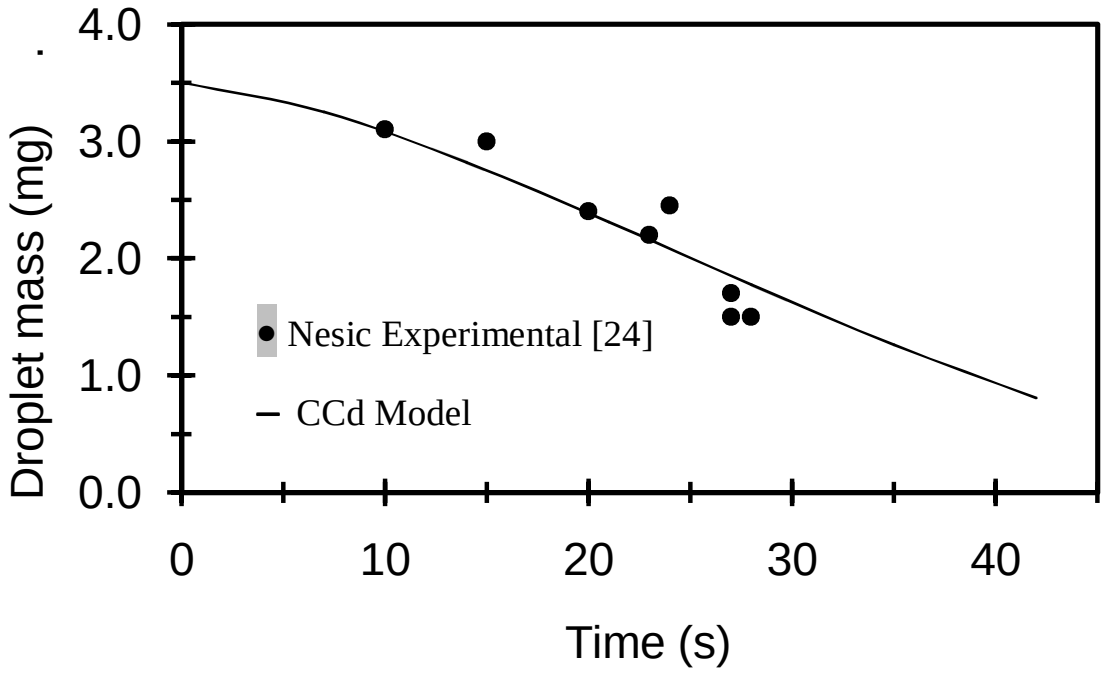

Figure 8. Experimental (Nesic [24]) vs. Predicted (CCd) Drying History of Colloidal Silica in Air at 178°C

In the upcoming results, evaporation and drying of $CuCl_2$ droplets under different initial conditions will be examined. The studies involve variable air temperature, humidity, velocity and initial water content in the droplet.

Assume a 1 mm initial droplet diameter in all cases, except in the case where the effects of initial droplet size on the evaporation rate are investigated. In this latter scenario, 1.0, 1.16 and 1.5 mm diameter droplets will be considered.

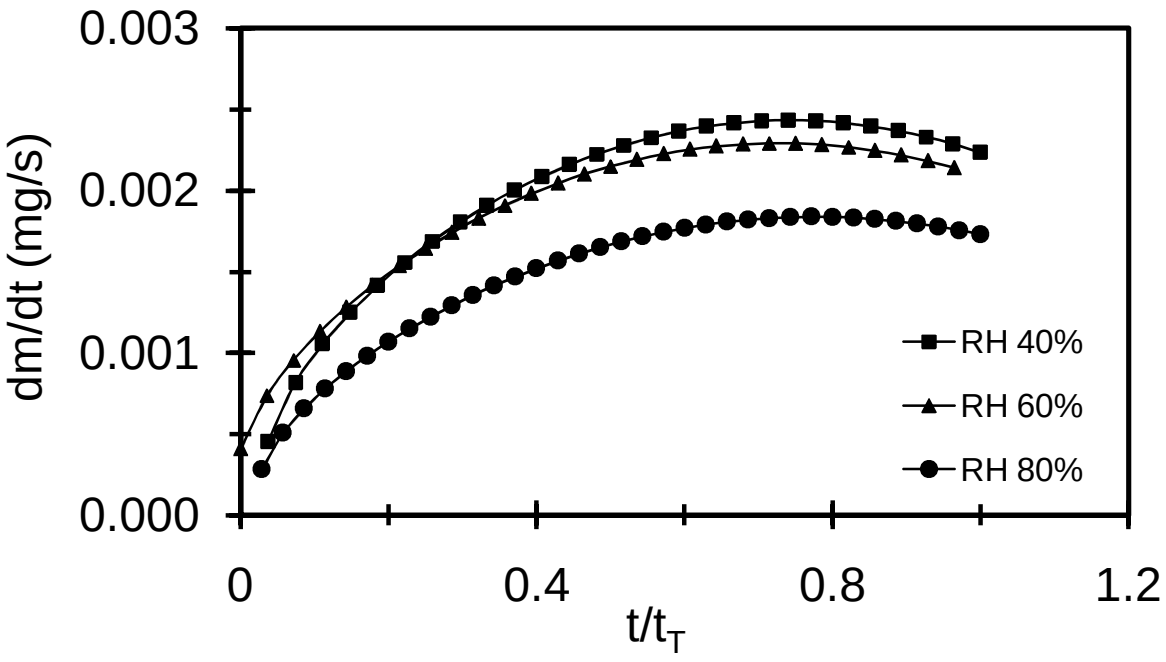

Figure 9. Droplet Evaporation Rate Vs. Changes in Relative Humidity of Air at T_{dp} = 75°C, V = 1.75 m/s, 3 mol H_2O, D_o = 1.0 mm

Figure 9 shows the predicted evaporation rate, when conditions are set at 75 ^{o}C in the air, and the RH is allowed to change between 40% and 80%. The curve shows an inflection point, indicating changes in the trend of the evaporation rate at fractions between 0.7 and 0.8 of the total evaporation time. Further analysis indicates that this inflection of the curve occurs near the critical humidity concentration of water in the droplet. As the ratio of solids versus water in the droplet increases, the evaporation rate is lower (a falling rate) and eventually decreases dramatically, thereby tending to negligible.

Past research tends to separate the drying process into constant and variable evaporation rate starting and finishing at different times. There is no clear agreement in the literature about when and why the evaporation rate changes. Xu [5] associated the change from a constant rate to decreasing or variable rates with the appearance of a crust on the surface of the droplet. The crust restricts the flow of vapor, from inside the droplet, and the evaporation rate becomes variable, with a decreasing intensity as the thickness of the crust increases.

Xu [5] evaluated the evaporation rate using the Reaction Engineering Approach and a Characteristic Drying Rate Curve. The results indicated a period of constant evaporation rate, followed by a drastic change once the critical ratio is reached. This period is called the falling evaporation rate period.

In general, the literature typically shows mass versus time changing in exponential or logarithmic manner, indicating the presence of a variable evaporation rate with time. The same processes produce graphics of evaporation rate versus humidity content that reflect a constant evaporation rate period followed by a well defined falling rate period. These observations are confirmed in Fig. 7.

Some authors believe that the variability of the evaporation rate depends on the formation of solid crust on the surface of the droplet, or that this happens because of the reduction of surface area, as a consequence of mass change. In Figures 9 and 12, the evaporation rate versus time is shown. The model indicates the presence of an evaporation rate that grows steadily with time. It becomes stagnant when the critical moisture content (X_c) is reached. At this point, which occurs around the time of $t/t_t = 0.8$, the mass transfer driving process reaches its limit and the evaporation rate starts to decrease.

The ratio m/m_o, defined as the ratio of the instantaneous droplet mass to the initial droplet mass, is used here to facilitate a comparison of curves when starting from different initial water concentrations of slurry.

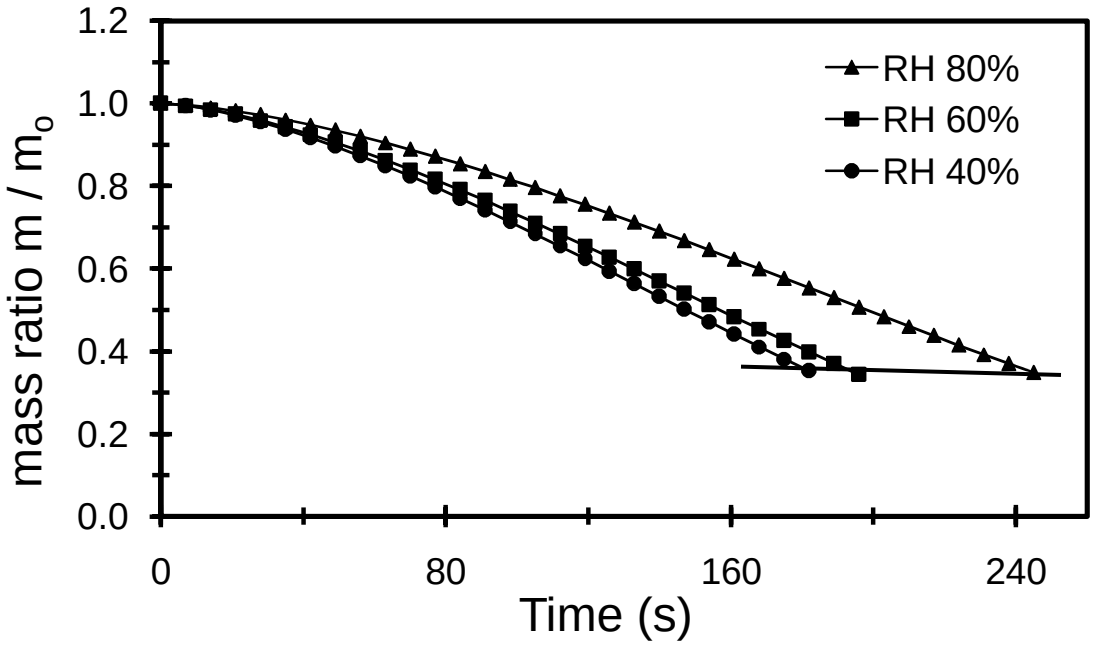

Figure 10. Mass Ratio Evolution with Time Using Air at 75^{o}C, D_o = 1.0 mm, V = 1.75 m/s

The effect of air humidity content on the drying time can be better seen from Fig. 10, where a droplet with an initial diameter of 1 mm, and initial composition of 3 mol water to 1 mol $CuCl_2$, is allowed to dry in air flowing at 1.75 m/s and 75^{o}C. At a higher humidity content in air, the absolute drying times tend to be longer, with a non-linear correspondence between the drying time and increased air humidity content. Of particular interest is the significant separation between the curves at 60% and 80% humidity, when compared to the 40% curve. At 80% RH in air, the constant drying rate period is shorter and the droplet drying occurs under a longer falling rate period. Under the three different air humidity conditions, the droplet reaches the critical mass at times where the mass ratios are similar.. After 100 seconds, the mass ratio is between 80% and 60%.

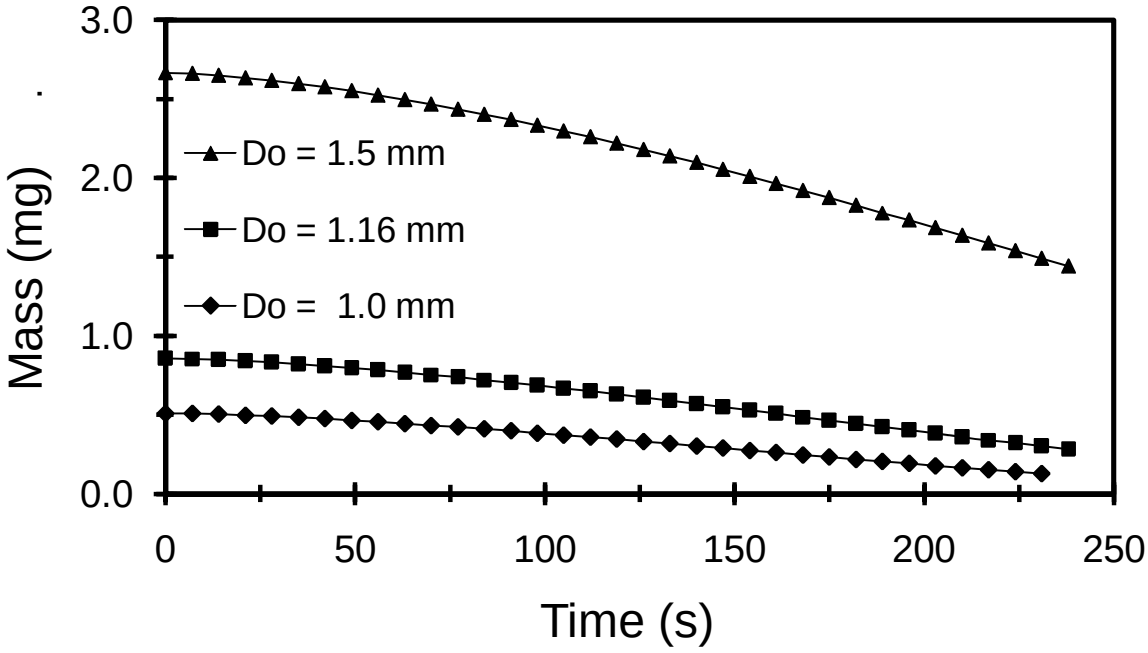

Figure 11. Change in Droplet Mass Vs. Time with Air at 75^{o}C, RH = 50%, HR = 0.14, T_{dp} = 59^{o}C, V = 1.75 m/s

Using time as a limiting variable, and starting from droplets with different compositions and sizes in contact with a drying medium under identical thermal conditions, different drying ratios are obtained. Maintaining constant air thermal characteristics provides useful information for extrapolation of droplet sizes and compositions to a common dryer geometry, for similar drying results. The process is simulated to the point where the droplet reaches its critical humidity ratio.

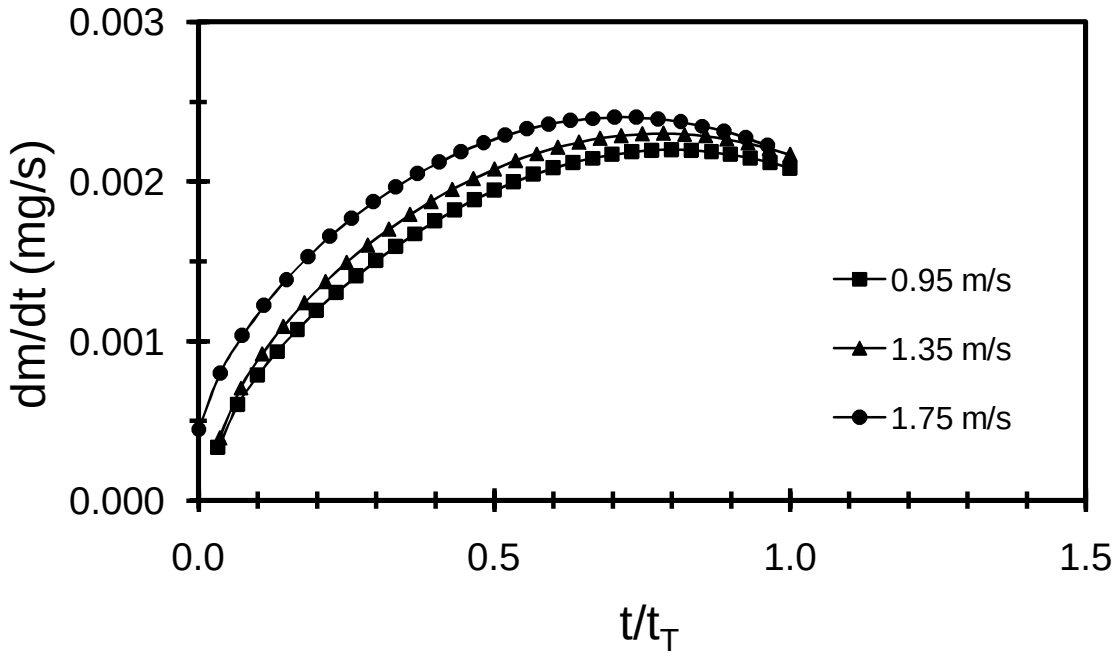

Figure 12. Effects of Air Velocity on the Evaporation Rate with Air at 75°C, RH = 50%, 3 mol H_2O, T_{dp} = 59°C, HR = 0.14 kg/kg, D_o = 1.0 mm

In Fig. 11, three droplets with initial compositions of 1, 3 and 5 mol H_2O and 1.5 mm, 1.16 mm and 1.0 mm diameter, respectively, are immersed in a drying medium at 75°C, 50 % RH and 1.75 m/s. With those initial diameters and under these, composition and air conditions, the droplets reach a critical mass at approximately similar times.

The evaporation rate predicted by the model has small changes for different air velocities. This observation was previously confirmed through experiments performed by Walton [2], Kadja [10] and Aguilar [12]. The model is based on the assumption of a continuous carrier phase (air) which permits the utilization of the Navier-Stokes Equations. When the size of

particles immersed in a the air stream is such that dimensions of the particle are comparable to the mean free path of molecules in the air, the assumptions of Navier-Stokes Equations are no longer valid. A non-continuum regime must be considered in that case where the velocity profile and mass transfer are influenced by the free molecular effect [15]. The ratio between the mean free path and a characteristic dimension of the flow geometry is commonly defined as the Knudsen number (Kn). The value of the Knudsen number provides an indication of the lack of influence of velocity on certain phenomena. As the velocity of air increases, the drag force imposed on the droplet is also higher. Given the small size of the droplet, it does not behave like a fixed surface in space and it "moves" with the continuous phase. The relative change in the evaporation rate that results from a velocity change becomes small and negligible. The process is fundamentally mass transfer driven, as opposed to heat transfer (convection) driven.

In Fig. 12, changing the velocity of air from 0.95 m/s to 1.75 leads to higher evaporation rate from a droplet of 1 mm initial diameter and 3 mol H_2O initial water content. The evaporation rate increases by approximately 10%, while the critical mass is reached with no substantial change at around 80% of the total drying time.

From the results shown in Fig. 13 to 16 it can be seen that the effects of increased air temperature lead to less drying time as the air temperature increases between 75^{o}C and 115^{o}C, for droplets containing initial water concentrations of 1, 3 and 5 mol H_2O. A 1 mol

H_2O particle with a 1 mm initial diameter reaches a critical mass in 120, 75, 60 and 45 seconds as the air temperature increases to 75, 95, 105 and 115^oC, respectively.

From the results in Fig. 13, the model shows that a lower drying rate occurs at a smaller water content, per each mol of $CuCl_2$. Assume a critical water content of 0.1 mol at which point the humidity content is 9.0% on a weight basis, or 0.065 mg in a 1 mm initial diameter droplet. With air at 75^oC, HR = 0.1 kg H_2O/kg air, and an initial water content of 1 mol H_2O, the droplet reaches its critical water content in about 110 seconds.

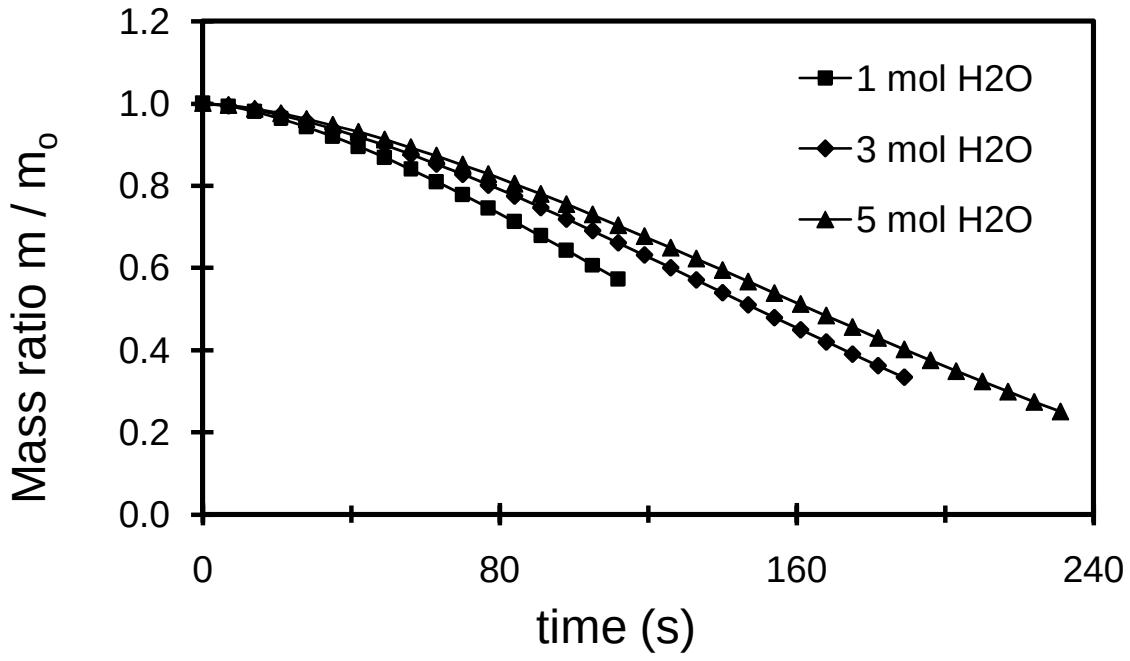

Figure 13. Mass Ratio Evolution Vs. Time with Air at 75^oC, RH = 50%, HR = 0.14 kg/kg, T_{dp} = 59^oC, D_o = 1.0 mm, V = 1.75 m/s

The total drying time increases from 110 *s* to 190 *s* and 240 *s*, when the initial water content is increased from 1 to 5 moles. The solution procedure converges well, provided the initial humidity stays lower than 10 moles water.

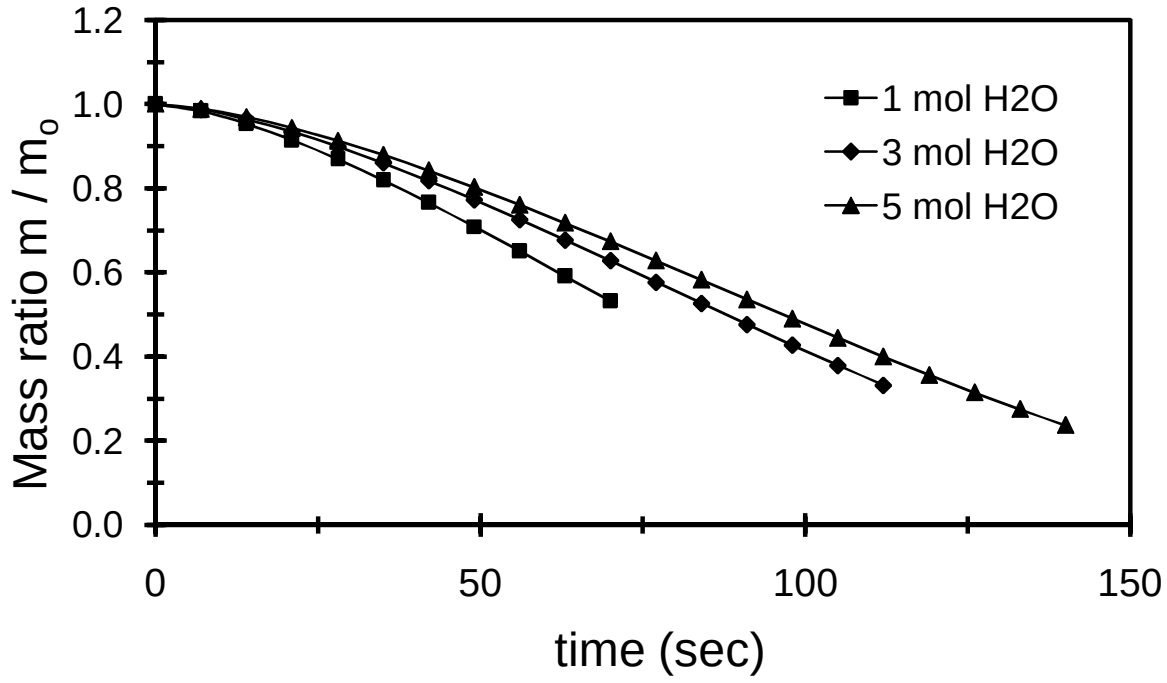

Figure 14. Mass Ratio Evolution with Air at 95^{o}C, RH = 50%, HR = 0.14 kg/kg, T_{dp} = 77^{o}C, D_o = 1.0 mm, V = 1.75 m/s

With air at 95^{o}C, the model results indicate a time reduction of 40 s, for a droplet with an initial water content of 1 mol, 80 s for a droplet with an initial water content of 3 mol, and 95 s for an initial water content of 5 mol. With other variables remaining constant, the impact of a higher temperature on reducing the drying time is more notable in droplets with an initial water content of 5 mol, because of a larger surface area.

For a droplet with an initial water concentration of 5 mol, the time required to reach the critical mass decreases from 5 s to 2 s per ^{o}C, as the air temperature increases from 75^{o}C to 115^{o}C. A droplet with a 1 mol initial water content takes 2 sec per ^{o}C with air at 75^{o}C, and 1 s per ^{o}C at 115^{o}C.

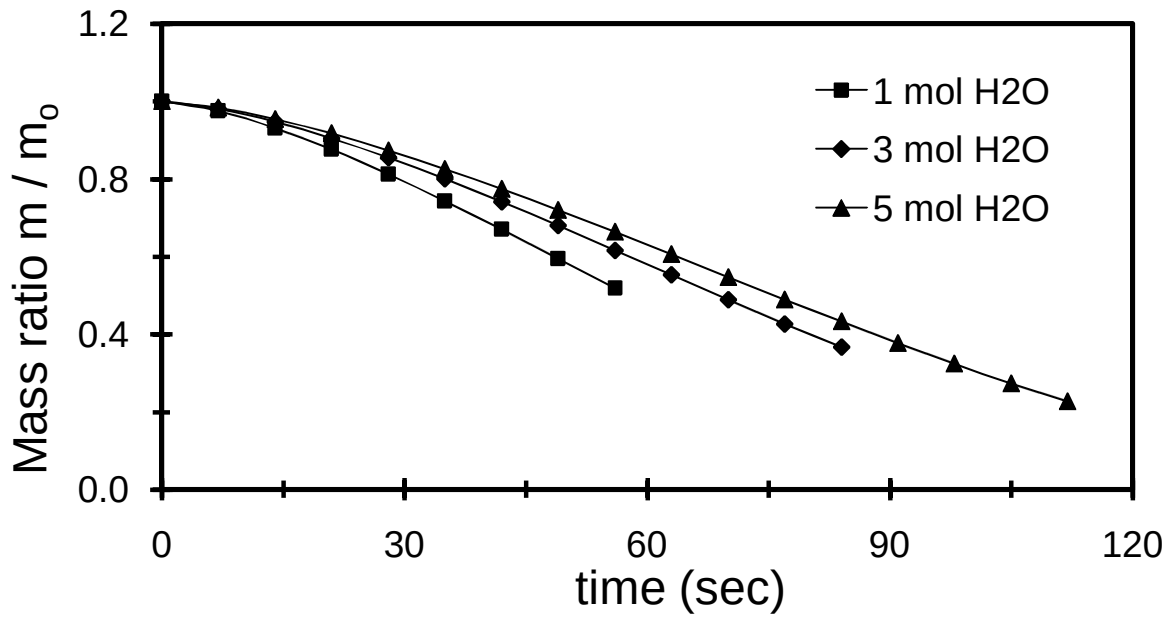

Figure 15. Mass Ratio Evolution at 105^{o}C, RH = 50%, HR = 0.14 kg/kg, T_{dp} = 86^{o}C, D_o = 1.0 mm, V = 1.75 m/s

The model indicates that a droplet with D_o = 1 mm requires 110 *s* to reach the critical humidity content, if allowed to dry in air at 75^{o}C and starting from 1 mol water content. The same time is required for droplets with an initial water content of 3 mol in air at 98^{o}C,

and 5 mol in air at 106°C. The resulting ratio of dry $CuCl_2$ powder, starting at 5 mol, is 1/3 when compared to that starting at 1 mol.

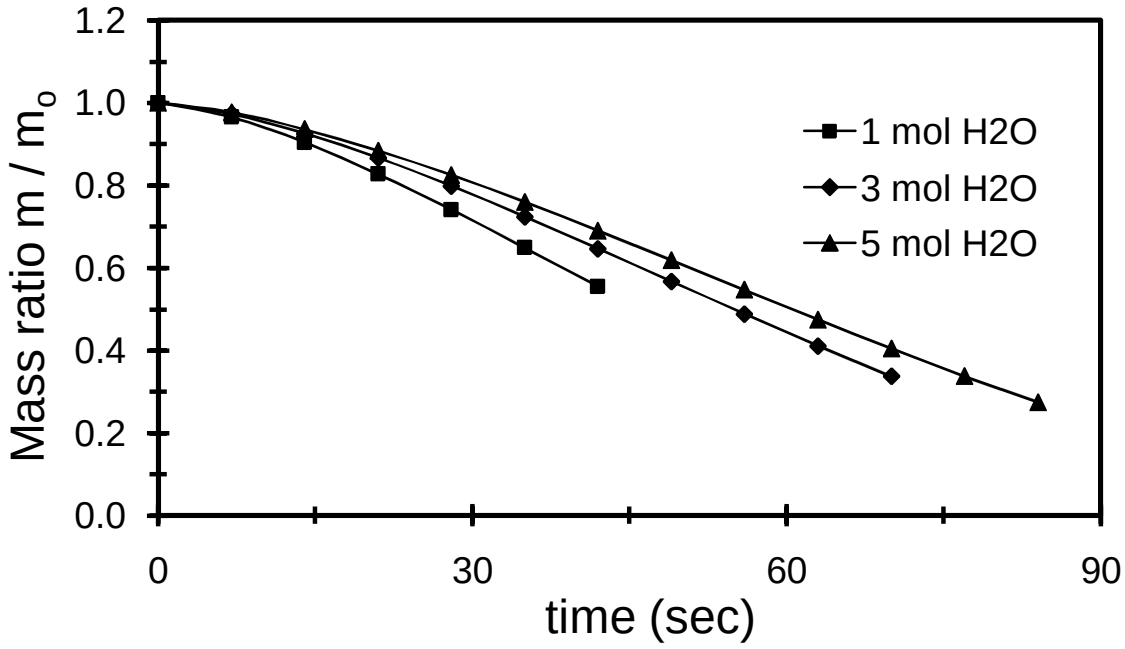

Figure 16. Mass Ratio Evolution Vs. Time with Air at 115°C, RH = 50%, HR = 0.14 kg/kg, T_{dp} = 95°C, D_o = 1.0 mm, V = 1.75 m/s

The net change of mass for a droplet with D_o = 1 mm and an initial water concentration of 1 mol is 3 times the initial mass. For a droplet with an initial water concentration of 5 moles, the change of mass is 6 times the initial mass. With a slurry water content increasing from 1 to 5 moles, the drying time more than triples. In practical applications, this information can help balance the energy compromise of removing water before spraying, and the energy required to heat air.

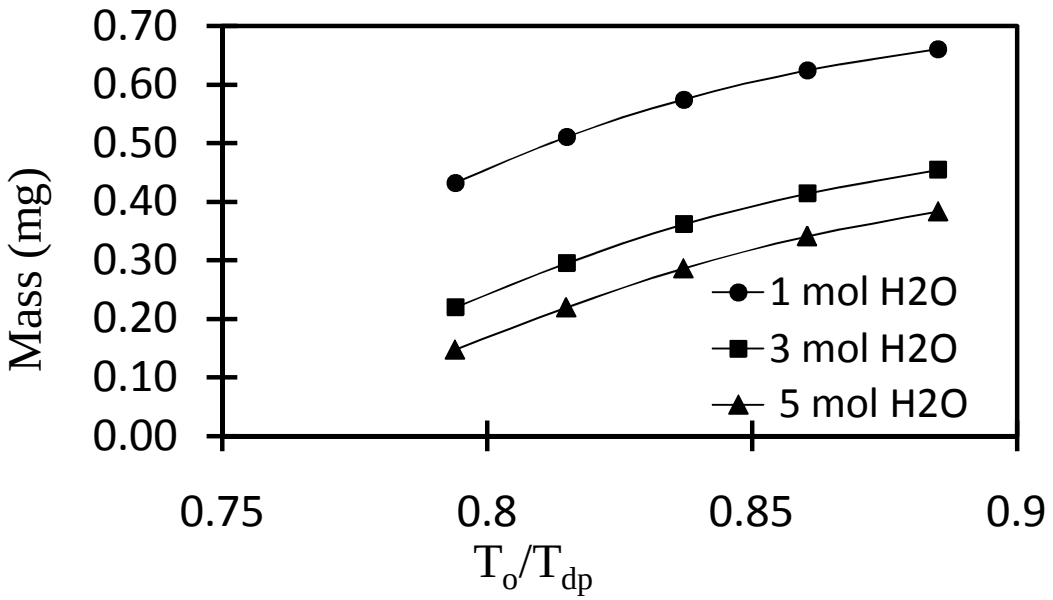

Figure 17. Droplet Mass Change vs. Ratio of Initial Droplet Temperature to Changing Air Temperature at RH = 50%, Do = 1 mm, V = 1.75

The model shows that the droplet mass behaves independently of the initial water concentration for different air temperatures. This effect can be seen from the almost parallel curves at 1, 3 and 5 mol initial water concentration in figure 17. This observation is important when considering the overall balance of energy of the process. The initial water content and temperature of the air do not change the process fundamentally. Other considerations such as the length of time of the drying process, size of the chamber and size of the dry particle, must be considered before setting the initial conditions of the slurry.

The $CuCl_2$ slurry is composed of a suspension of small solid particles in a spherical liquid droplet. Unbound water evolves at a temperature corresponding to the saturation

temperature at atmospheric pressure. The results have shown the evaporation and shrinkage of a particle with mostly unbound water (up to 80%) in a dry air stream at constant thermodynamic conditions. The droplet reaches the air wet bulb temperature, before the mass transfer process begins.

There is an approximately linear relation between drying times for a droplet with initial water contents varying from 1 to 5 mol of H_2O. Whit air temperature going from 75^oC to 115^oC, the drying time for a 1 mol water content droplet varies from 40s to 100s. The magnitude of change in total time grows as the amount of initial water in the droplet is increased to 5 mol H_2O. This relationship can be seen from figure 18.

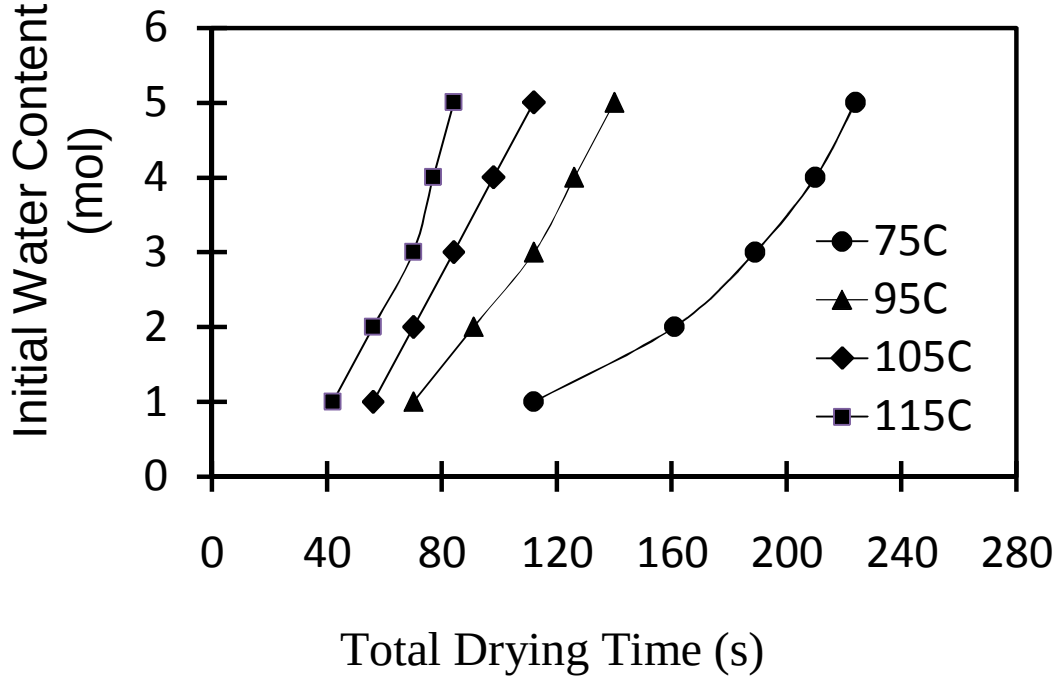

Figure 18. Initial Water Content Vs. Total Drying Time with Air Temperatures of 75^oC, 95^oC, 105^oC and 115^oC

5.0 Conclusions and Recommendations for Future Research

5.1 Conclusions

This thesis has shown a potential for utilization of low-grade (low temperature) heat in the drying process of $CuCl_2$ slurry, opening the possibility for the utilization of waste heat as low as 70^oC from industrial or nuclear sources. At the lowest temperature of the air, assuming an initial concentration of 3 moles H_2O, a droplet of diameter 1.0 mm will dry in approximately 140 seconds. If the initial water content is 1 mol, the drying time falls to about 90 seconds.

Spraying of small droplets of $CuCl_2$, in the range of 1.0 mm diameter and concentrations between 1 and 5 mol H_2O, was examined for low temperature air. The formulation provides a useful design tool to determine the ideal drying conditions, requiring minimum energy consumption.

Further analysis of the predictions indicated that extreme values of the drag coefficient between 0.6 and 2 do not lead to changes of the drying rate. They partially explain the small effect of velocity in the results. This is expected given the mass transfer driven nature of the process.

Preheating and pressurizing the slurry to produce flashing upon atomization did not result in substantial benefits. In a flashing process, the main factor of the drying process is primarily the size of the rained-out droplets. Thus, the process becomes a standard process of evaporative spray drying.

The analysis determined the magnitude of the evaporation rate under constant air flow conditions, starting from a concentrated slurry of $CuCl_2$ and water. The focus of the analysis is low temperature air, with initial droplet temperatures down to 70^oC. The temperature of the $CuCl_2$ solution from the electrolyser is between 80^oC and 100^oC and it is allowed to cool down to 35^oC. The results suggested that the initial droplet temperature does not produce a substantial effect on the drying rate. By allowing the solution to cool down to 35^oC or lower, the benefit of precipitating solids and making the mechanical removal of water possible, leads to shorter drying times and smaller equipment.

It was observed that the concentration of the aqueous slurry has an impact on the size of the resultant particles. This is consistent with the assumption that the critical water content of the droplet does not change with concentration.

Eslamian et al. [15] concluded that the initial concentration of the droplet has no impact on the resultant morphology of the particle. The sphericity or natural crystal shape is constant regardless of the initial water content. Following the findings by Eslamian et al.[15], the present study did not consider the morphology of the resulting substance. Langrish et al.[6]

demonstrated that the drying rate curves for the same material at different operating conditions should be geometrically similar. This research confirms the hypothesis from results obtained from the mathematical model. The $CuCl_2$ drying curves maintain similarity with variations of velocity, humidity, temperature and droplet properties.

5.2 Recommendations for Future Research

This thesis focuses on the effect of critical parameters of initial water content of the droplet, air temperature and air humidity. The results indicate a strong relationship between those parameters and provide light on the design of experimental chambers. An immediate consequence is the need to understand the net energy requirements of the process. The initial slurry concentration and the final humidity content of particles have a great impact in the overall energy requirements. In particular, the final humidity of $CuCl_2$ particles can have considerable impact in the efficiency of a thermo-chemical process for the production of hydrogen. An energy analysis that considers this interaction is necessary to get a better understanding of the impact of drying $CuCl_2$ in the overall process. This should help determine if alternative drying processes must be considered together with the possibility of using other sources to heat air.

References

[1] G. F. Naterer, V. N. Daggupati, G. Marin, K. Gabriel, Z. Wang, Thermo-chemical Hydrogen Production with a Copper-Chlorine Cycle, II: Flashing and Drying of Aqueous Cupric-Chloride**.** University of Ontario Institute of Technology, Oshawa, Ontario, Canada, 2008

[2] D. E. Walton, The evaporation of water droplets. A single droplet drying experiment, Drying technology, 22 (2004) 431–456

[3] H. Salman, M. Soteriou, Lagrangian simulation of evaporating droplet sprays United Technologies Research Center, East Hartford, Connecticut, Volume 16, number 12, December 2004

[4] W. E. Ranz & W. R. Marshall, Jr., Evaporation from drops. Parts I & II.Chem. Eng. Program. 48:141-6; 173-80, 1952. University of Wisconsin, Madison.

[5] S. Xu, Q. Lin, X. Chen, A Model for Drying of an Aqueous Lactose Droplet Using the Reaction Engineering Approach, Drying Technology, 24 (2006) 1329–1334

[6] T. A. G. Langrish, T. K. Kockel, The assessment of a characteristic drying curve for milk powder for use in computational fluid dynamics modeling, Chemical Engineering Journal 84 (2001) 69–74

[7] X. D. Cheng, S. Xu, Q. Lin, Air drying of milk droplet under constant time dependent conditions, Food and bio-Product processing cluster, The University of Auckland, New Zealand. DOI 10.1002/aic.10449, April 11, 2005

[8] L. Huang, M. L. Passos, K. Kumar, A. S. Mujumdar, A Three-Dimensional Simulation of a Spray Dryer Fitted with a Rotary Atomizer Drying Technology, 23 (2005) 1859–1873

[9] J. Wang, R. G. Evans, Drying behavior of droplets of mixed powder suspensions Journal of the European Ceramic Society, 26 (2006) 3123–3131

[10] M. Kadja, G. Bergeles, Modelling of slurry droplet drying, Applied Thermal Engineering 23 (2003) 829–844

[11] M. Mezhericher, A. Levy, I. Borde, Theoretical Drying Model of Single Droplets Containing Insoluble or Dissolved Solids, Drying Technology, 25 (2007) 1035–1042

[12] G. Aguilar, B. Majaron, W. Verkruysse, Y. Zhou, J. S. Nelson, E. J. Laverna, Theoretical and experimental analysis of droplet diameter, temperature and evaporation rate evolution in cryogenic sprays, International Journal of Heat and Mass Transfer 44 (2001) 3201-3211

[13] J. Yang and S. Wong, An Experimental and Theoretical study of the effects of heat conduction through the support fiber on the evaporation of a droplet in a weakly convective flow. International Journal of Heat and Mass Transfer, 45 (2002) 4589-4598

[14] L. Huang and A. S. Mujumdar, Simulation of an Industrial Spray Dryer and Prediction of Off-Design Performance, Drying Technology, 25 (2007) 703–714

[15] M. Eslamian, M. Ahmed and N. Ashgriz, Modelling of Nanoparticle formation during spray pyrolysis. Nanotechnology, 17 (2006) 1674-1685

[16] H. Fu-Yu, W. H. Liau, Evaporation of solution droplets in spray pyrolysis. International Journal of Hat and Mass Transfer, 41 (1998) Nos 8-9, 993-1001

[17] M. Farid, A new approach to modeling of single droplet drying, Chemical Engineering Science, 58 (2003) 2985-2993

[18] K. C. Patel, X. D. Chen, S. Kar, The Temperature Uniformity During Air Drying of a Colloidal Liquid Droplet Drying Technology, 23 (2005) 2337–2367

[19] V. S. Birchal, L. Huang, A. S. Mujumdar, M. L. Passos, Spray Dryers: Modeling and Simulation, Drying Technology, 24 (2006) 359–371

[20] G. Brenn, Concentration Fields in Drying Droplets, , Chemical Engineering Technology 2004, 27, No 12. DOI 10.10002/ceat.200407025

[21] V. Cleary, P. Bowen, H. Witlox, Flashing liquid jets and two-phase droplet dispersion I. Experiments for derivation of droplet atomization correlations, Journal of Hazardous Materials 142 (2007) 786-796

[22] D. L. Chang, C. Fon, F. Lee, Development of a simplified bubble growth model for flash boiling sprays in direct injection spark ignition engines, Proceedings of The Combustion Institute, 30 (2005) 2737-2744

[23] K. Asano, Mass Transfer, from fundamentals to modern industrial applications, Wiley-VCH, ISBN 3-527-31460-1, 2006

[24] S. Nesic´, The evaporation of single droplets—Experiments and modeling. In Drying'89; Mujumdar, A.S., Ed.; Hemisphere: New York, 1990 386–393.

[25] G. F. Naterer, Heat Transfer in Single and Multiphase Systems. CRC Press, ISBN 0849310326

[26] M. Rahman, R. Verhoeven and C.A. Brebbia, Advances in Fluid Mechanics *IV*, Eds. WIT Press, ISBN: 1-85312-910-0

[27] W. Liu, D.C. McPhail, Thermodynamic properties of Copper-Chloride complexes and copper transport in magmatic-hydrothermal solutions, Chemical Geology 221 (2005) 21–39

[28] The Engineering Tool Box 2005. Air Properties. [Online], Retrieved Dec 22, 2007 from http://www.engineeringtoolbox.com/air-properties-d_156.html

Appendix A

The following Matlab routine produces shows the iteration algorithm for the droplet Equation, with a marching method to obtain the diameter versus time solution.

```
function h=humidity(Tdb, RH, Mwair, MwH2O)
%This function calculates the vapor concentration in the bulk air Cg, and
%the vapor concentration at the droplet surface Cs.
%R=gas constant
R=8.314;
%Air pressure, Pa
Pa=103000
%Saturated partial vapor pressure at Tdb, Pa
A=10^(7.5*Tdb/(237.7+Tdb));
Psdb=6.11*A;
%Wet bulb temperature calculation, deg oC
Twb=237*log(Psdb*RH/611)/(7.5-log(Psdb*RH/611));
%Saturation pressure at the droplet surface, Pa
B=10^(7.5*Twb/(237.7+Twb));
Psds=6.11*B;
%Humidity Ratio HR
HR= 0.62198*Psdb/(Pa-Psdb);
%Moisture fraction in air
Xi=(HR/MwH2O)/(1/Mwair+HR/MwH2O);
%Vapor concentration in air
Cg=Xi*Pa/(R*(273.3+Tdb));
%Vapor concentration at droplet surface
Cs=Psds/(R*(273.3+Twb));
```

```
%Droplet,
%Calculates the results of the expanded Taylor series, based on
%local parameters of humidity, temperature and pressure; and droplet
%parameters of concentration and critical humidity.
clear;
Vnet=input('enter net velocity   ')
Do=input('initial droplet diameter     ')
N =input('initial mol H2O       ')
Tdb=input('dry bulb temperature air C     ')
RH=input('Relative humidity air %     ')
MfrCuCl2= 1/(N+1);
MfrH2O=N/(N+1);
%Ncr=Moles of water beyond which the drying rate becomes a falling rate;
Ncr=0.1;
RoCuCl2=3300;
RoH2O=990;
%Molecular weight CuCl2;
MwCuCl2=0.134;
%Molecular Weight H2O;
MwH2O=0.018015;
%Molecular weight Air
Mwair=0.02801;
Roavg=RoCuCl2*MwCuCl2 +RoH2O*MwH2O;
g=9.8;
Roair=0.97447;
a= g+g*(Roair/Roavg);
muair=2.07e-5;
b=75*(muair/Roair)/(Do)^2;
```

```
P=b*Vnet;
Q=b/3+Vnet;
epsilon=1e-6;
Xdevi=1;
%Diffusivity coefficient of vapor in air
Dv=2.91e-5;
massdr=[];
mH2O=1;
mCuCl2=1;
Xcr=MwH2O*Ncr/MwCuCl2*1;
n=100;
t=0;
while Xdevi >= epsilon;
  for i=1:1:n;
    h=feval(@humidity, Tdb, RH, MwH2O, Mwair);
    J=-4*Dv*N*(h)/Roavg;
    t=t(i);
    Do=Dnew;
    Vt=Vnet+P*t+Q*t^2;
    fy=-J*Do^-2-0.5*(K*Do^-1.5)*(Vn+P*t+Q*t^2)^0.5;
    Dfirst=J*Do^-1+(K*Do^-0.5)*Vn^0.5;
    Dsecond=(0.5*K*Do^-0.5)*(Vnet^-0.5)*(P+2*Q*t)+fy*Dfirst;
    DthirdA=-0.25*K*Do^-0.5*((Vnet+P*t+Q*t^2)^-1.5)*(P+2*Q*t)^2;
    DthirdB=(0.5*K*Do^-0.5)*((Vnet+P*t+Q*t^2)^-0.5)*(2*Q);
    DthirdC=(2*(-0.25)*(K*Do^-1.5)*((Vnet+P*t+Q*t^2)^-0.5)*(P+2*Q*t))*Dfirst;
    DthirdD=fy*Dsecond+(2*J*D^-3+(0.75*D^-2.5)*(Vnet+P*t+Q*t^2)^0.5)*Dfirst^2;
    Dthird=DthirdA+DthirdB+DthirdC+DthirdD;
    Dd=Do+Dfirst*fy+(Dsecond*t^2)/2+(Dthird*t^3)/6;
    massdr=(Roavg*3.14159*Dd^3)/6;
    %Xcr=mH2O/mCuCl2
```

```
    Xcr=(MwH2O*Ncr)/(MwCuCl2*1);
    %Xnew=mH2O/mCuCl2;
    %massdr=mH2O+mCuCl2;
    %mH2O=massdr-mCuCl2;
    Xnew=(massdr/(MwCuCl2*1))-1;
    massdr=(Xnew+1)*(MwCuCl2*1);
    Roavg=massdr/((3.14159*Dd^3)/6)
  end
    massdr=[massdr Dd];
    Xdevi=abs(Xcr-Xnew);
end
  iterations=i;
  plot(t, massdr)
```